NASA CONTRACTOR REPORT

NASA CR-112030

A PERFORMANCE APPLICATION STUDY OF A JET-FLAP HELICOPTER ROTOR

By: R. J. Sullivan, Sally LaForge, and Barry W. Holchin

National Aeronautics and Space Administration
Langley Field, Virginia

Prepared Under Contract No. NAS 1-10365 by
HUGHES TOOL COMPANY - AIRCRAFT DIVISION
Culver City, California
for Langley Research Center

NATIONAL AERONAUTICS AND SPACE ADMINISTRATION • WASHINGTON, D.C. • MAY 1972

NASA CR-112030

A PERFORMANCE APPLICATION STUDY OF A JET-FLAP HELICOPTER ROTOR

By R. J. Sullivan, Sally LaForge, and Barry W. Holchin

National Aeronautics & Space Administration
Langley Field, Virginia

Prepared under Contract No. NAS 1-10365 by
HUGHES TOOL COMPANY - AIRCRAFT DIVISION
Culver City, California

for Langley Research Center

NATIONAL AERONAUTICS AND SPACE ADMINISTRATION

FOREWORD

This study was performed by the Technical Department of the Hughes Tool Company-Aircraft Division, under the direction of K. B. Amer, Manager, Technical Department. Principal investigators included:

Project Engineer & Propulsion	R. J. Sullivan	Senior Staff Engineer
Program planning & integration & Aerodynamics	Sally LaForge	Chief, Performance & Computer Programming Section
Computer programming	B. W. Holchin	Senior Programmer
Weight Analysis	E. Vega	Chief, Weights Section

CONTENTS

CONTENTS (continued)

CONTENTS (continued)

Page No.

TABLES:

Contents (Continued)

A PERFORMANCE APPLICATION STUDY OF A JET-FLAP HELICOPTER ROTOR

SUMMARY

A performance study was made of the application of a jet-flap to a reaction-drive rotor for a heavy-lift helicopter mission and for a high-speed-helicopter maneuverability (200 knots, 2g) mission. The results of the study are as follows:

Heavy Lift Helicopter Mission

As a result of the increase in maximum airfoil lift coefficient achieved by the jet-flap, rotor solidity is reduced with the jet-flap to approximately 59% of a non-jet-flap rotor.

As a result of the saving in rotor solidity, and hence in rotor weight, the jet-flap configuration had a 21% higher productivity than a non-jet-flap configuration.

Of the three propulsion systems studied utilizing a jet-flap (Hot Cycle, Warm Cycle, Cold Cycle) the Hot Cycle gave the largest increase in productivity.

200 Knot 2g Mission

The 200 knot 2g mission is performed best with a Warm Cycle propulsion system. The jet-flap permits designing for a rotor blade loading coefficient $C_T/\sigma = .170$ at 2g without encountering blade stall. A conventional rotor will allow a C_T/σ of only .083 at 200 knots. Thus, the jet-flap rotor permits a 200 knot 2g maneuver without suffering the penalty of an unreasonable rotor solidity that would be required by a non-jet-flap rotor.

INTRODUCTION

The concept of applying a jet-flap to a helicopter rotor to improve performance has received attention for several years.

In the case of the jet-driven rotor, it is necessary to integrate the internal gas thermodynamics, the external blade aerodynamics, and the blade structural and dynamics design requirements. Studies of the jet-flap helicopter on a jet-driven rotor (such as Reference 1) concluded there was no clear-cut total system cost advantage of the jet-flap helicopter over shaft-driven helicopters for high speed and heavy lift missions. The present study is intended to provide additional information on the potential performance advantage of the jet-driven helicopter equipped with a jet-flap.

The study has two objectives, each related to widely different vehicles and missions. The initial work is concerned with a heavy lift mission, which has a cruise speed, with payload, of 110 knots. The objective of the first part of this study is to employ a jet-flap on a helicopter rotor so as to obtain the largest improvement in productivity, compared to a reference warm cycle, no-jet-flap helicopter. By the nature of the jet-flap, more lift is derived by the integration of the airfoil aerodynamics and the propulsion system flow than by dealing with aerodynamics and propulsion separately, and blade stall effects in the usual sense can be postponed to a more heavily loaded condition. This means that the helicopter can simply be flown faster than usual with a conventional blade chord (or solidity). Alternately, if speed is limited to a certain value as was done in this Heavy Lift study, the blade chord can be reduced substantially below the conventional size, thus reducing rotor weight, profile power, and hopefully, fuel. As a goal, a 50% reduction in rotor solidity was sought, corresponding to a doubling of the rotor (C_T/σ) from the usual .10-.11 to .20-.22.

In the case of the second mission investigated, the objective was to determine whether a conventional solidity pure helicopter with a jet-flap rotor can perform the desired mission of sustained 2g at 200 knots. A later study should be considered of the optimum helicopter configuration to perform the 200 knot, 2g mission, in order to evaluate the place of the jet-flap helicopter.

SYMBOLS

A	rotor disk area, ft^2, πR^2
A_D	rotor blade duct area, in^2
A_1	lateral cyclic blade pitch angle, deg; positive is blade leading edge down at Ψ = 0 deg.
A_π	helicopter parasite drag area, ft^2
a	speed of sound, ft/sec Also, lift curve slope
a'	longitudinal tilt of thrust vector, deg; positive aft
B	rotor blade tip loss factor, .97 for jet-flap rotor
B_1	longitudinal cyclic blade pitch angle, deg; positive is blade leading edge down at $\Psi = 90^o$
b	number of blades
C_d	total local section drag coefficient, $\frac{d}{q_\ell c}$
C_{d_o}	drag coefficient due to section shape (no jet effects)
$C_{d_{MF}}$	drag coefficient due to mechanical flap
C_H	rotor longitudinal force coefficient, $\frac{H}{\rho A(\Omega R)^2}$
C_ℓ	total local section lift coefficient, $\frac{\ell}{q_\ell c}$
C_{ℓ_o}	lift coefficient due to section shape (no jet effects)
C_{L_R}	rotor lift coefficient, $\frac{L}{\rho A(\Omega R)^2}$
C_{P_P}	propulsive power coefficient, $\frac{A_\pi q V_f}{A\rho(\Omega R)^3}$

C_Q rotor torque coefficient, $\frac{Q}{A\rho(\Omega R)^2 R}$

$C_{Q_{COR}}$ coriolis torque coefficient, $\frac{bW_a}{A\rho(\Omega R)g}$

$$\bullet\left[x_i^2 + \sum_{i=2}^{5}(x_i^2 - x_{i-1}^2)\left(1 - \sum_{j=1}^{i} K_j\right)\right]$$

$C'_{Q_{Noz}}$ tip nozzle torque coefficient, $\frac{W_a K_5 V_5 b}{gA\rho(\Omega R)^2}$

C_T rotor thrust coefficient, $\frac{T}{\rho A(\Omega R)^2}$

C_T/σ blade loading coefficient

C_{V_e} effective nozzle velocity coefficient

C_{X_R} rotor propulsive force coefficient, $\frac{X}{\rho A(\Omega R)^2}$

c blade chord, ft (aerodynamics); in (weights)

c_j local section momentum coefficient, $\frac{mV_j}{q_\ell c}$

D_e diverter valve exit diameter, in

D_H duct hydraulic diameter, ft

DWN rotor download on fuselage/rotor thrust

d total local section drag per unit span, lb/ft

EW empty weight, lb

e flapping hinge offset, ft

f	duct friction coefficient
GW	gross weight, lb
g	acceleration of gravity, ft/sec^2
H	downwind force perpendicular to shaft, lb
I_h	blade inertia moment about flapping hinge, $slug\text{-}ft^2$
i_{Noz}	incidence of tip nozzle to blade tip, deg; positive up
j	numbering variable for jet-flap sections (j=1,4) and tip nozzle (j=5)
K	state-of-the-art weight improvement factor Also, ratio of specific heats
K_j	fraction of gas flow leaving an element of the flap-nozzle region
L	lift, lb
ℓ	total local section lift per unit span, lb/ft
M_c	centrifugal force moment about flapping hinge, ft-lb
M_D	duct Mach Number
M_I	blade inertia moment about flapping hinge, ft-lb
M_T	blade thrust moment about flapping hinge, ft-lb
M'_W	blade weight moment about flapping hinge, ft-lb
M_x	local Mach Number on blade surface
m	jet mass flux per unit span, all blades, $\frac{slugs}{sec\text{-}ft}$
N_e	number of engines (=3)
N_t	number of fuel tanks
P	local gas pressure, lb/in^2

P_{air}	rubber engine air flow expressed as a fraction of reference engine air flow, $W_a/W_{a_{ref}}$
P_{amb}	ambient pressure, lb/in^2
P_e	engine exhaust pressure, lb/in^2
P_2	engine inlet pressure (including ram), lb/in^2
PL	payload, lb
(P.L.)	engine power level
PPF	ratio of profile drag of a blade section to that for a NACA 0015
Q	rotor torque, ft-lb
q	free stream dynamic pressure, lb/ft^2
q_ℓ	local dynamic pressure, $\frac{1}{2}\rho U^2$, lb/ft^2
R	blade radius, ft
R_G	gas constant, $\frac{ft\text{-}lb}{lb_m\text{-}^oR}$
r	distance from blade flapping hinge to blade station, ft
S	surface area, ft^2
S_d	supercirculation thrust parameter, see equation (B-2)
S_ℓ	supercirculation lift parameter, see equation (B-1)
T	rotor thrust, lb Also, local gas temperature, ^oR
T_e	engine exhaust temperature, ^oR
T_{DRAG}	engine air ram drag, lb
T_2	engine inlet temperature, ^oR or ^oF

t	blade thickness at deepest section, in
U	local velocity perpendicular to blade span, ft/sec Also, $\frac{\text{blade duct area}}{\text{blade cross-section area}}$
U_P	component of U along the shaft axis
U_T	component of U perpendicular to shaft axis
u	dimensionless local velocity, $U/\Omega R$
V	free-stream velocity, ft/sec
V_B	helicopter block speed, $\frac{\text{mission radius}}{\text{total time}}$, knots
v	induced velocity, ft/sec
V_j	local jet velocity, ft/sec
V_T	rotor tip speed, ft/sec, ΩR
V_t	max redline tip speed, ft/sec In Weight Equations, V_t = 750 (Heavy Lift) = 700 (High Speed)
V_5	nozzle jet velocity, ft/sec
W_a	design engine air flow, lb/sec
$W_{a_{ref}}$	engine air flow for reference engine (Table 1), lb/sec
W_g	design gross weight, lb Also, engine gas flow, lb/sec
W_{g_b}	design gross weight of baseline helicopter, 105,000 lb
X	propulsive force, positive upstream, lb
x	dimensionless radial station, r/R

α_S rotor angle of attack, deg

α_P blade element angle of attack, deg

$\alpha_{(1)(270)}$ retreating blade tip angle of attack, deg; see Appendix C

β blade flapping angle with respect to shaft, positive upward, deg

Γ flow function $\frac{N_e W_g \sqrt{T_e}}{b P_e A_D} = f(M_D)$

γ' blade Lock Number, $\frac{c\rho a R^4}{I_h}$

δ jet deflection, positive downward from chordline, deg

Θ_o blade root pitch, deg

Θ_1 blade twist, positive up at tip, deg

Θ_{CAM} simulated blade camber on inboard portion of blade, deg

$\lambda o, \lambda$ inflow ratio, $\frac{V \sin \alpha - v}{\Omega R}$

μ tip speed ratio $\frac{V \cos \alpha}{\Omega R}$, also $\frac{V}{\Omega R}$

ρ free-stream air density, slugs/ft^3

σ rotor solidity, $\frac{bc}{\pi R}$

Ψ azimuth station, from rear in direction of rotation, deg

Ω rotational velocity of rotor, rad/sec

$\frac{W_A \sqrt{\theta}}{\delta}$ engine referred airflow, lb/sec

$\frac{W_F}{\delta\sqrt{\theta}}$	engine referred fuel flow

Weight Subscripts

arm	Armor/armament
ac	Airconditioning
ag	Auxiliary gear
ai	Air induction
an	Anti-icing
apu	Auxiliary powerplant
av	Avionics
B	Fuselage (body)
div	Diverter valve
e	Weight empty
el	Electrical group
es	Exhaust system
eng	Engine
fc	Flight controls
fe	Furnishings and equipment
fp	Fixed propulsion (engine controls and starter)
fs	Fuel system
fuel	Fuel for primary mission (fuel for warmup, hover, cruise, and reserve)
g	Gross weight
h	Hydraulics and pneumatics
i	Instruments
ir	Infrared countermeasure device

jd	Jet drive
lg	Alighting gear
ll	Winch lifting load
nac	Nacelle
pa	Passenger accommodations
r	Main rotor
rb	Rotor brake
re	Reference engine
tr	Tail rotor
ts	Tail surfaces
uf	Unusable fuel
ul	Useful load
w	Winch system
yfd	Yaw fan drive

DEVELOPMENT OF JET-FLAP BLADE DESIGN

The use of a jet-flap on a jet-driven rotor requires design integration of the propulsion, aerodynamic, and dynamic systems. Design work on blade structural configurations disclosed the possibility of using a honeycomb-type construction, leading to a simpler blade design than that previously employed in hot gas ducted systems. This honeycomb-type construction is discussed in Reference 2 and is shown in Figure 1.

A variation of this basic blade structural design is proposed for the jet-flap rotor blade considered here. It is proposed that the inboard portion of the rotor blade will not have a jet-flap, and that the outboard portion of the blade (outer 30-40 percent) will be equipped with a mechanically-actuated flap, of approximately 12.5% chord, as shown schematically in Figure 1.

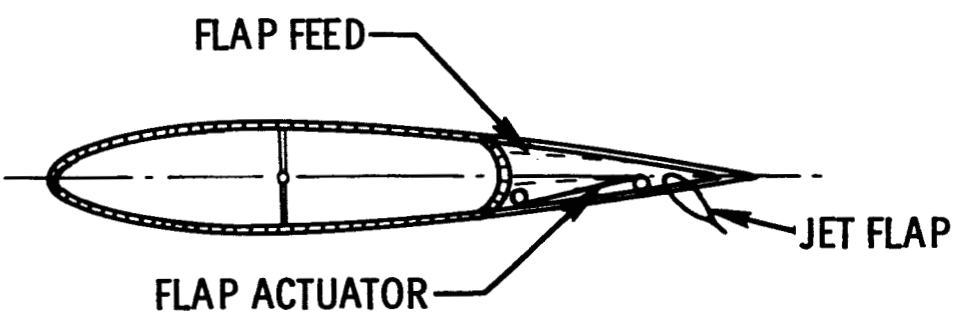

Figure 1. Schematic of Blade Construction and Jet Flap Installation

COMBINED PARAMETRIC DESIGN/PERFORMANCE PROGRAM

An analysis of the large number of interrelated design parameters of a gas-driven rotor system requires a parametric design program which incorporates a performance analysis, propulsion analysis, and weight analysis. The introduction of the jet-flap requires substitution of an aerodynamics performance program that is sensitive to the local changes in lift coefficient and drag coefficient brought about by the blowing action of the jet-flap.

An available performance program, organized in a numerical integration form, and based on the analyses presented in Reference 3 and 4 was combined with a parametric design program. This integrated program then permitted the investigation of various propulsion systems (hot, warm, and cold cycles), missions (heavy lift and high speed) and jet-flap parameters (percent gas bleed to flap, flap length/radius, flap deflection, etc.). In the execution of any one mission study, the performance routine is used several times, so computational time is longer than usual for a parametric program. However, by varying one parameter at a time (insofar as possible), an optimum helicopter configuration could then be defined for each mission.

Mission Definitions

The following two missions were selected to show the potential advantages of the jet-flap in applications of general interest.

Heavy Lift Helicopter

1.	Payload	30 tons (approx)(sea level, 95°F)
2.	Mission radius (payload both ways)	50 n miles
3.	Hover power requirement	500 fpm vertical rate of climb at 4000 feet, 95°F.
4.	Cruise speed	110 knots at sea level, 95°F
5.	Hover time per mission	20 minutes at sea level, 95°F
6.	Warm-up fuel allowance	500 pounds
7.	Reserve fuel	10% of initial
8.	Rotor tip speed	700 feet/second

High speed maneuverable (200 knot, 2g) helicopter

1.	Payload	3 tons (approx)(sea level, 95°F
2.	Mission radius (payload both ways)	100 n miles
3.	Hover power requirement	500 fpm vertical rate of climb at 4000 feet, 95°F
4.	Cruise speed	200 knots at sea level, 95°F
5.	Maneuver capability at 200 knots	2.0g
6.	Hover time per mission	5 minutes at sea level, 95°F
7.	Warm-up fuel allowance	75 pounds
8.	Reserve fuel	10% of initial
9.	Rotor tip speed	650 feet/second

Basic helicopter parameters

1.	Duct area utilization	U = .73
2.	Duct friction coefficient	f = .003
3.	No. of engines	3
4.	Jet-flap thrust recovery factor *	0.5

Discussion of Computer Program

An abbreviated program flow diagram of the parametric design/performance program is given in Figure 2. Special attention is given to the aerodynamics/performance subroutine. This part of the program calculates rotor forces and moments by numerical integration of blade element forces and moments. It should be noted that the introduction of the jet-flap did not increase the calculation time for a converged point, compared to a conventional, no-jet-flap case.

A detailed description of the equations used is found in Appendix A. Comments on the function of the performance subroutine formulation at the noted option location on Figure 2 are as follows:

* As defined by the term S_d, supercirculation thrust parameter, in Reference 5.

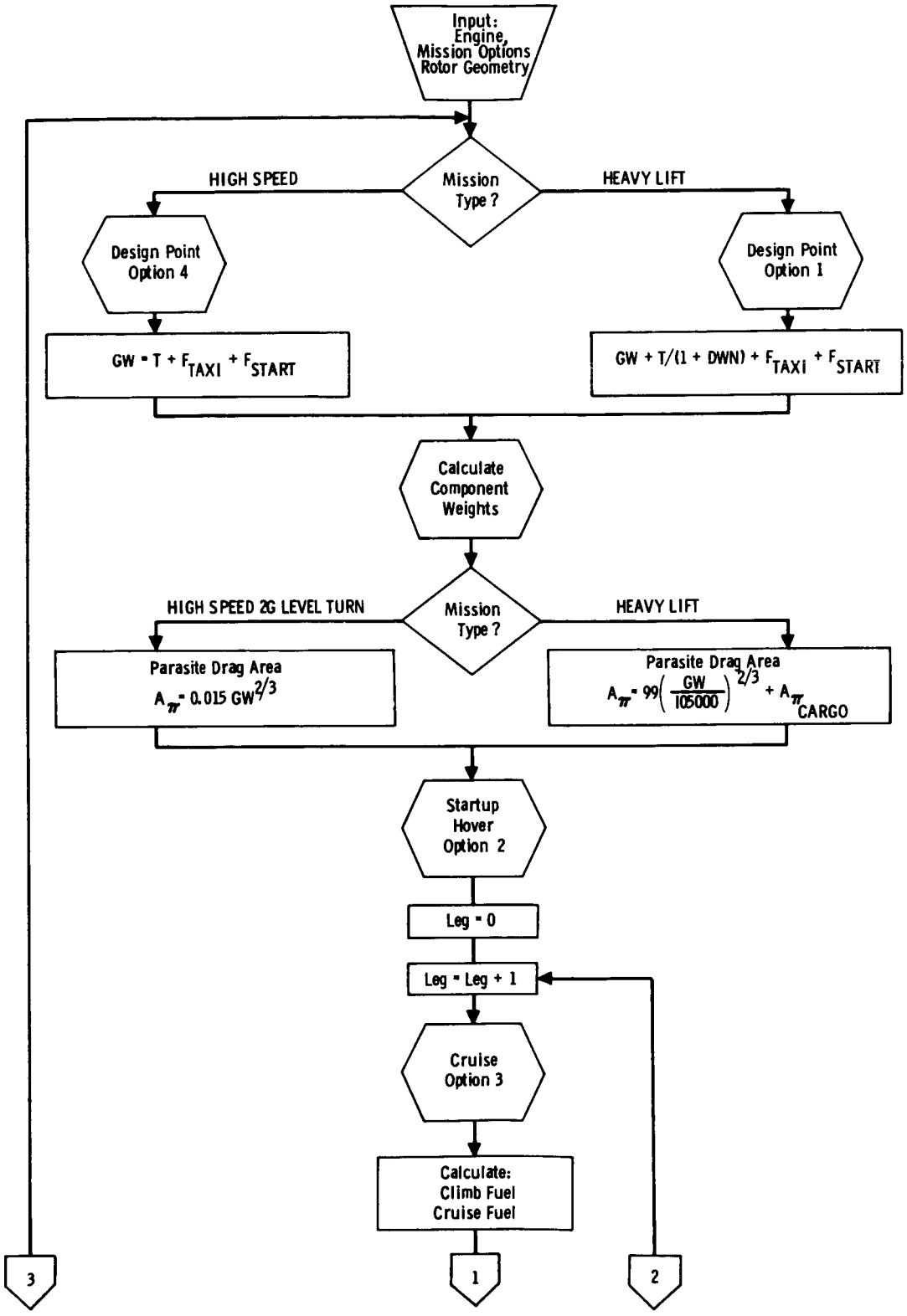

Figure 2. Computer Program Flow Diagram

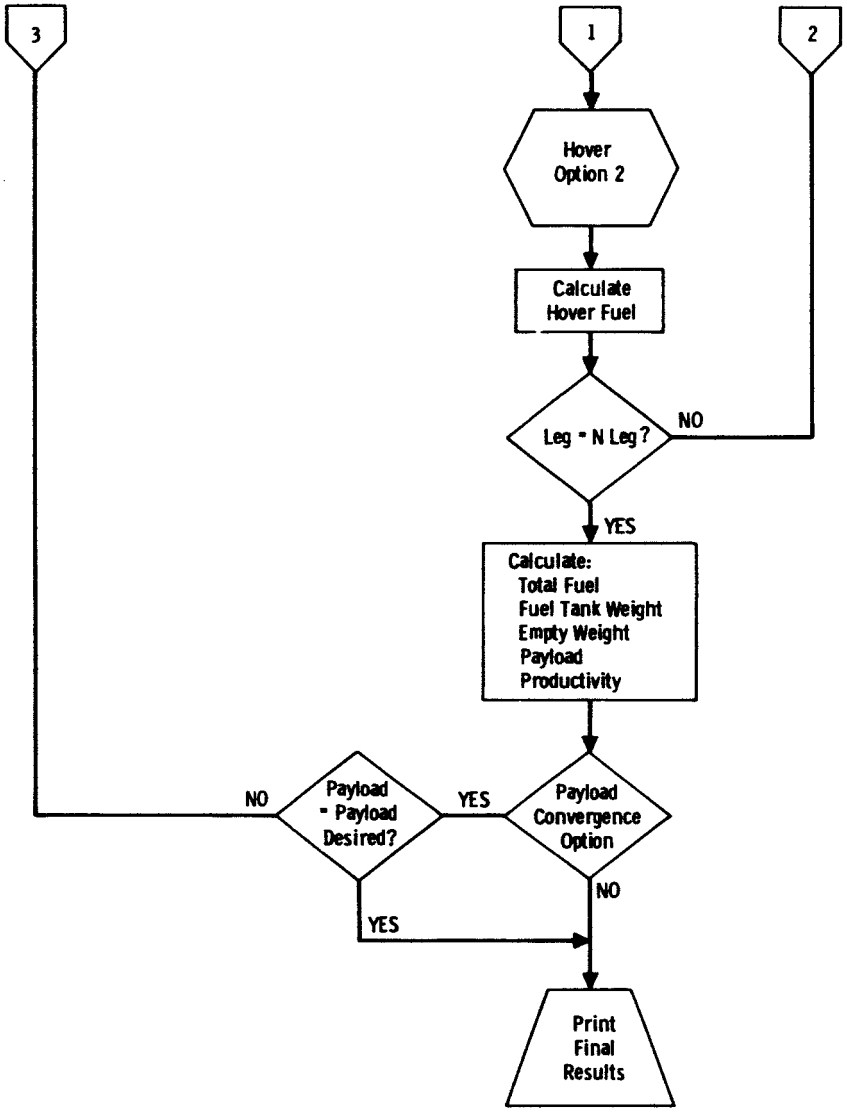

Figure 2. Computer Program Flow Diagram (Concluded)

Option 1. Heavy Lift design gross weight.- At zero airspeed, at a given vertical rate of climb, and at an engine power level (P.L.)*, inflow ratio (λo) and blade root pitch angle (θ_o) are varied from initial estimates until total rotor torque coefficient (C_Q) is zero and final vertical rate of climb equals the initial value.

Option 2. Hover fuel at a given gross weight.- Given a vertical rate of climb (including 0=hover) and rotor thrust (T) at zero airspeed, θ_o and (P.L.) are varied from initial estimates until C_Q equals zero and C_T equals the C_T calculated from the rotor thrust.

Option 3. Calculation of cruise fuel.- Total helicopter parasite area (A_π) and rotor thrust (T) are input at a given airspeed. These are converted to nondimensional form (C_{P_P} and C_T) by the following equations:

$$C_{P_P\ \text{input}} = \frac{A_\pi q V_f}{A\rho(\Omega R)^3} \tag{1}$$

$$C_{T\ \text{input}} = \frac{T}{A\rho(\Omega R)^2} \tag{2}$$

Then, λ_o, θ_o, and (P.L.) are varied until C_Q equals zero and the calculated values of C_{P_P} and C_T equal the input values. The parasite power coefficient $C_{P_{P\ \text{calculated}}}$ is determined as follows at the end of each iteration:

$$C_{P_{P\ \text{calculated}}} = \frac{C_T V_f}{(\Omega R)} \sin(-a' - \alpha_s) \tag{3}$$

$$\text{where } a' = \tan^{-1}\left(\frac{C_H}{C_T}\right) \tag{4}$$

$$\text{and } \alpha_s = \tan^{-1}\left(\frac{\lambda_o}{\mu} + \frac{C_T}{2B^2\mu^2\sqrt{1 + \left(\frac{\lambda_o}{\mu}\right)^2}}\right) \tag{5}$$

* See below for derivation of engine power level, (P.L.)

C_H and C_T are computed as shown in Appendix A. Since power level (P.L.) is also determined in the convergence process, cruise fuel flow can also be found.

Option 4. High speed design gross weight (200 knots, 2g).- Given A_π and (P.L.) for some airspeed, A_π is converted to non-dimensional form ($C_{P_{P\ input}}$). Then λ_o and θ_o are varied until C_Q equals zero and $C_{P_{P\ calculated}}$ equals $C_{P_{P\ input}}$. After the first iteration, A_π is recalculated during each iteration using the following empirical equation (6), (from Reference 6) where the T is available from the previous iteration.

$$A_\pi = .015\ T^{2/3} \tag{6}$$

Rotor Power Available and Power Level (P.L.)

The rotor power available (and power level, (P.L.) is determined by calculating the changes in pressure and temperature of the gas as it travels from the engine to the nozzles located either in the jet-flap region or the blade tip. The velocity is found from the pressure and temperature at the jet-flap segment or the tip nozzle. The velocity, together with the mass flow existing at the flap segment or the tip nozzle, produces a partial rotor driving torque. The partial torques are then integrated, and converted into total rotor power available.

Because of the specialized nature of the thermodynamic calculations which determine the gas pressure and temperature changes, a discussion is presented in Appendix B giving significant details of the power available calculation. Particular attention is given to the Mach Number variation down the blade, because Mach Number is the most significant variable in the change of pressure and temperature of the gas. The process described in Appendix B applies to all the gas entering the blade, and as far down the blade as the jet-flap. When the gas is bled to the nozzles of the jet-flap segments, the blade duct area is assumed to be reduced to maintain the Mach Number of the on-going gas as if no bleed had occurred. This duct area reduction is brought about by reducing the blade aerodynamic thickness ratio from typically .20 at the inboard end of the jet-flap to .15 at the outboard end, in order to minimize blade profile losses. After the rotor power available is determined by the procedures described here and in Appendix B, the engine power level (P.L.) discussed earlier is found as follows:

$$\text{Power Level} = (\text{P.L.}) = \frac{\text{Rotor Power Available}}{\text{Normal Rated Power}} \quad (7)$$

This parameter (P.L.) can have values in the range from .3 to about 1.4, depending on whether some low cruise power or takeoff (military) power is being considered.

It should be noted that, in all of the above options involving forward speed, engine ram drag (T_{DRAG}) is calculated as a function of engine power level (P.L.) by use of the following equation:

$$T_{DRAG} = \frac{W_a V_f}{g} \quad (8)$$

where W_a is total engine airflow (lbs/sec). This parameter is converted to an equivalent flat plate area and added to the parasite area, A_π, and is used in equation (1) each time (P.L.) is changed.

Jet-Flap Aerodynamic Characteristics

The jet-flap aerodynamic characteristics used in this study are presented in Appendix C. These characteristics include lift coefficient vs momentum coefficient, section drag coefficient, stall angle of attack, limit angle of attack, and thickness effects on drag.

Empty Weight Determination

The discussion of determination of empty weight is presented in Appendix D. Empirically-derived equations are presented for the several empty weight components for the Heavy Lift and for the high speed helicopters.

Propulsion System Configurations

It was pointed out earlier that acceptable jet-flap aerodynamic performance can be obtained independently of whether or not a hot, warm, or cold supply of blowing gas is used. It does require a complete helicopter preliminary design study to determine whether a whole helicopter is a more efficient design using various types of gas supply. Because of the broad nature of the study here, and in the interests of consistency, a relative comparison was made of three types of propulsion systems, called the Warm Cycle, the Hot Cycle, and the Cold Cycle. A schematic of the three alternate systems is given in Figure 3.

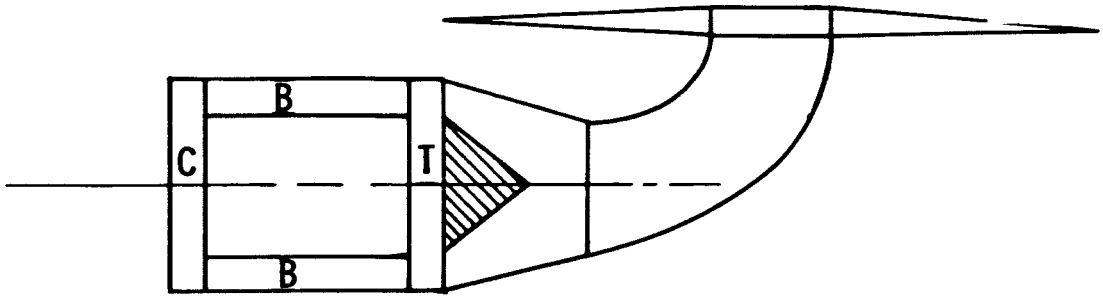

a) HOT CYCLE (Turbojet

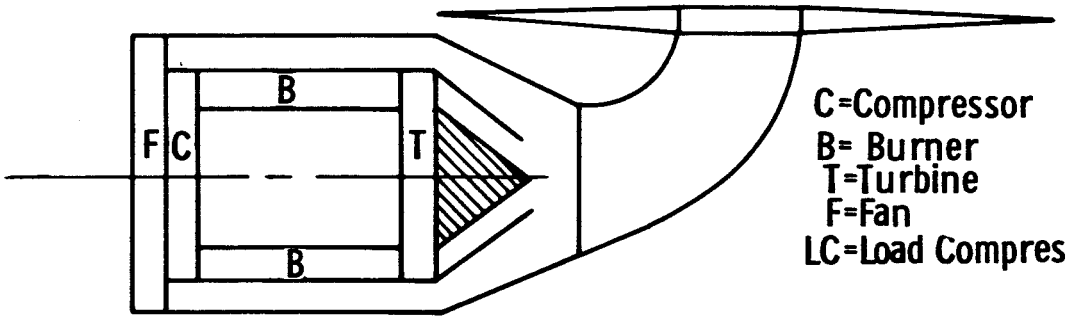

b) WARM CYCLE (Low Bypass Turbofan

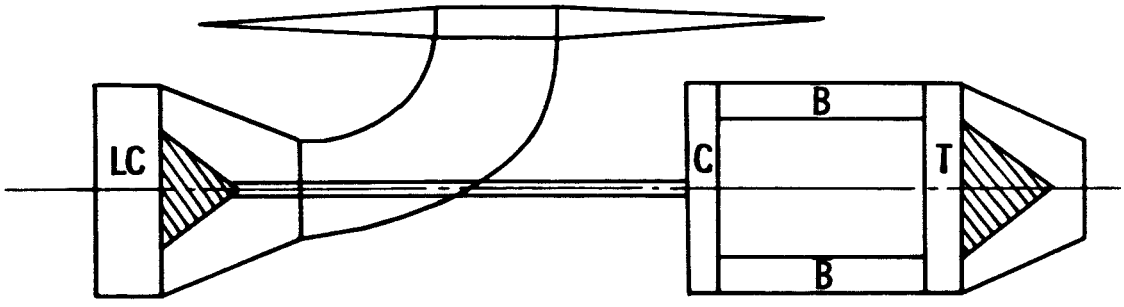

c) COLD CYCLE (Turboshaft Plus Load Compressor

Figure 3. Propulsion System Configurations

Warm Cycle.- The Warm Cycle engine was the keystone of the study, and is essentially a low bypass turbofan engine of high compression ratio (>20:1), with cooled turbine blades.

As used here, the fan and core gas streams are collected in a common tailpipe and permitted to mix as rapidly as possible to a homogeneous pressure and temperature as shown in Figure 3b. Mixing losses for pressure and temperature were based on engine manufacturers' calculations and test, and all Warm Cycle rotor performance calculations were based on complete mixing. Table 1 gives the pressure ratio, temperature, airflow, fuel flow, and weight for the rubberized Warm Cycle engine used in this study.

Hot Cycle.- Information was gathered to determine the nature of the unmixed fan and core gas streams of current advanced technology low bypass turbofan engines, as well as the resulting mixed stream properties, for a range of power settings from Military rating to Idle power. With this information, a calculation was made to determine the amount of energy supplied to the bypass fan, and to convert that energy to a higher pressure and temperature associated with a pure turbojet (zero bypass ratio) engine of the same overall compression ratio, turbine inlet temperature, core airflow, and fuel flow (see Figure 3a) The "rubberized" Hot Cycle engine characteristics are given in Table 1. Because the Hot Cycle engine is much simpler than the Warm Cycle in that it has no turbine blading to drive a bypass fan nor any bypass fan, it is substantially lighter than the Warm Cycle. It does produce substantially higher pressure and hotter gas, which affects blade design; however, the substantial blade chord reduction possible with the Hot Cycle system compared to the lower pressure Warm Cycle makes the Hot Cycle a very attractive candidate system.

Cold Cycle.- The Cold Cycle system as shown in Figure 3c can be seen to be essentially a turboshaft conversion of the Hot Cycle gas generator engine, with a load compressor to supply compressed air to drive the rotor and operate the jet-flap.

Thus, the compressor pressure ratio can be chosen independently of the basic engine cycle, and thus (as also happens with the Hot Cycle) the gas can be made so dense that the blade duct requirement (for the Heavy-Lift mission) will be reduced to the point that conventional aerodynamic limits rather than any thermodynamic limits will set the blade chord. In addition, the Cold Cycle discharge temperature is lower than that of the Hot Cycle or the Warm Cycle, making the blade design problem easier.

The gas conditions associated with the Hot Cycle in Table 1 will produce a shaft power specific fuel consumption of under 0.4 lbs per hour per shaft horsepower, and will also develop a specific

power of approximately 180 shaft horsepower per pound of air per second. In the scheme proposed in Figure 3C, this type of turboshaft engine is connected to a load compressor of the axial type with a design point efficiency of 0.875, and a design pressure ratio of 6.5 to 1. A generalized compressor map was used, taken from Reference 7, and part load performance of the compressor was matched to the part power performance of the equivalent turboshaft engine. It was found that the load compressor will deliver 1.2 pounds per second for each pound per second of gas generator core flow; therefore, the Cold Cycle system used here has a "bypass ratio" of 1.2 to 1.0. The design point performance of the rubberized Cold Cycle system is also in Table 1.

Rubberized engine characteristics.- The following characteristics are all based on a common core of fixed overall compression ratio, turbine inlet temperature, and air flow.

TABLE 1

RUBBERIZED ENGINE CHARACTERISTICS (SEA LEVEL; 59°F)

Cycle	Warm	Hot	Cold
Reference Engine Air Flow- lb/sec - $W_{a_{ref}}$	250	154	184
Gas pressure ratio-P_e/P_{amb}	3.0	4.4	6.4
Temperature - °F	900	1380	500
Fuel Flow - lb/hr	10500	10500	10500
Weight - lb.	2300	1700	3100

This table shows that the same core engine is used throughout this study, because all three engine types have the same fuel flow.

Criteria for Comparison of Configurations

The basic criterion for comparison of the several configurations was chosen to be specific productivity.

$$\text{PRODUCTIVITY} = \frac{\text{PAYLOAD X BLOCK SPEED}}{\text{EMPTY WEIGHT}} \qquad (9)$$

This parameter is chosen because it appears to represent helicopter cost effectiveness (performance vs cost) better than other criteria such as minimum gross weight for a mission.

(It is noted that, in this study with an essentially fixed payload and fixed block speed, highest productivity is obtained with the lowest empty weight).

Fuel/payload* ratio is a frequently-mentioned optimization parameter. It is presented in the Tables for the interested reader, and typical fuel/payload curves are given in Figures 6a and 7a for information purposes. The justification for using productivity for optimization is given in Appendix E.

RESULTS OF THE HEAVY-LIFT MISSION JET-FLAP STUDY

The purpose of this study was to find the vehicle configuration and propulsion system which gave the best jet-flap performance (Productivity) and compare that vehicle with a reference no-jet-flap vehicle. The three jet-flap propulsion systems described above were the Hot Cycle, Warm Cycle, and Cold Cycle. The propulsion system selected for the reference no-jet-flap vehicle was the Warm Cycle because preliminary work showed that best performance (Productivity) would be obtained with the Warm Cycle. To illustrate, the Warm Cycle productivity (4 blades) was 108.8** and the Hot Cycle productivity (4 blades) was 96.7, about 11% lower.

The tables and charts below describe the process of elimination to obtain the best configuration. The tables and charts showing the effect of the parametric variables are examples taken from designs where comparable data were available and are not necessarily the selected optimum designs.

Reference Warm Cycle (No-Jet-Flap)

A brief set of Warm Cycle - no-jet-flap cases were run to establish reference performance against which to measure performance gains from use of the jet-flap. A four bladed rotor***with 15% airfoil thickness was used, and initially, a disk loading of approximately 10.0 pounds per square foot was sought. Results are shown below in Table 2 and Figure 4 for the influence of duct Mach Number.

* $\frac{\text{Fuel}}{\text{Payload}} = \frac{W_{\text{fuel}}}{\text{Payload}}$

** Figure 5

*** See Appendix F for discussion of number of blades for baseline vehicle.

TABLE 2

WARM CYCLE - NO-JET-FLAP - EFFECT OF DUCT MACH NUMBER (CHORD)

Duct Mach Number	.355	.406	.447
C - in.	58.0	55.4	53.9
R - ft.	61.75	61.60	61.75
σ	.0997	.0953	.0927
Disk Loading-lb/ft^2	10.09	10.08	10.07
% Engine Airflow - P_{air}	.453	.463	.474
Payload - tons	30.09	30.02	29.91
Productivity	107.7	108.6	108.6
C_T/σ *	.1076	.1125	.1155
$\alpha_{(1.0)(270)}$ Margin-deg **	4.51	3.94	3.58
W_g - lb	120533	120270	120328
Fuel/Payload	.2157	.2224	.2303

Figure 4 shows that in the Mach Number range from .35 to .45 that the highest productivity (108.7) is obtained at a duct Mach Number of about .42. The rotor C_T/σ is approximately .114.

Additional cases were then run at a Mach Number of .42 for a range of disk loadings, and the results are shown in Table 3 and Figure 5.

* Tabulated C_T/σ is for 4000 feet, 95^{o}F. For sea level, 59^{o}F, multiply by 0.808.

** See Appendix C for discussion of limit angles of attack (margin).

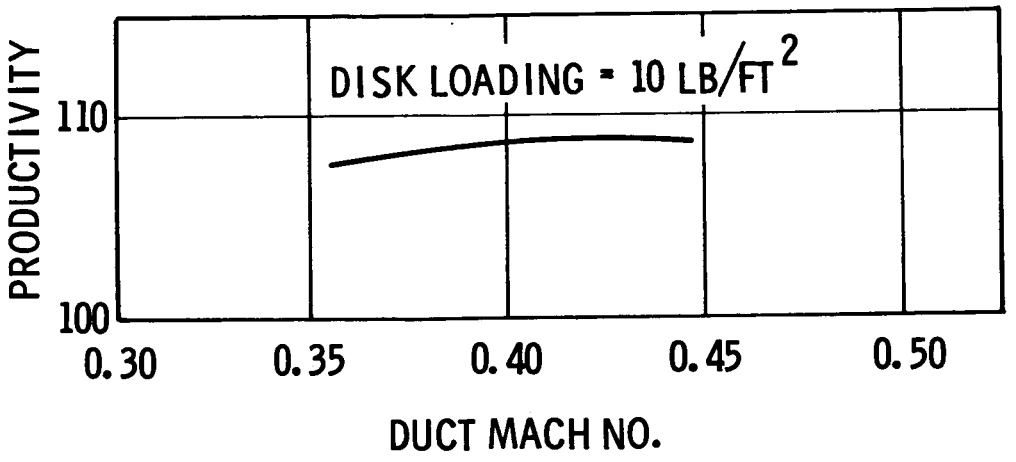

Figure 4. Warm Cycle - No Jet Flap - Effect of Duct Mach Number on Productivity

TABLE 3

WARM CYCLE - NO-JET-FLAP- EFFECT OF DISK LOADING (BLADE RADIUS)

Disk Loading - lb/ft^2	9.00	10.08	11.08
R - ft	65.30	61.75	58.90
C - in	53.6	54.7	55.7
σ	.0871	.0904	.1004
Duct Mach Number	.424	.425	.423
% Engine Airflow - P_{air}	.449	.469	.484
Payload - tons	30.03	30.02	29.91
Productivity	108.4	108.7	108.7
C_T/σ	.1098	.1140	.1173
$\alpha_{(1.0)(270)}$ Margin-deg	4.36	3.76	3.27
W_g - lb	120226	120433	120382
Fuel/Payload	.2194	.2257	.2319

Figure 5 shows that, in the disk loading range from 9 to 11 pounds per square foot, the highest productivity is 108.8, at a disk loading of 10.3 pounds per square foot, with C_T/σ = .115. Productivity = $\frac{PL \times V_B}{EW}$ = 108.8 is taken as the reference no-jet-flap value. Fuel/payload is .23.

Hot Cycle Propulsion System

As was mentioned earlier, the Hot Cycle propulsion system was found (in screening calculations) to give the highest performance. Therefore, the broadest study of jet-flap parameters was applied to the Hot Cycle, with results noted below. The variables are discussed in the order of their general importance, rather than the order in which they actually were studied. Relative engine size (% engine airflow) was varied to maintain approximately 30 tons payload over the range of the variable of interest.

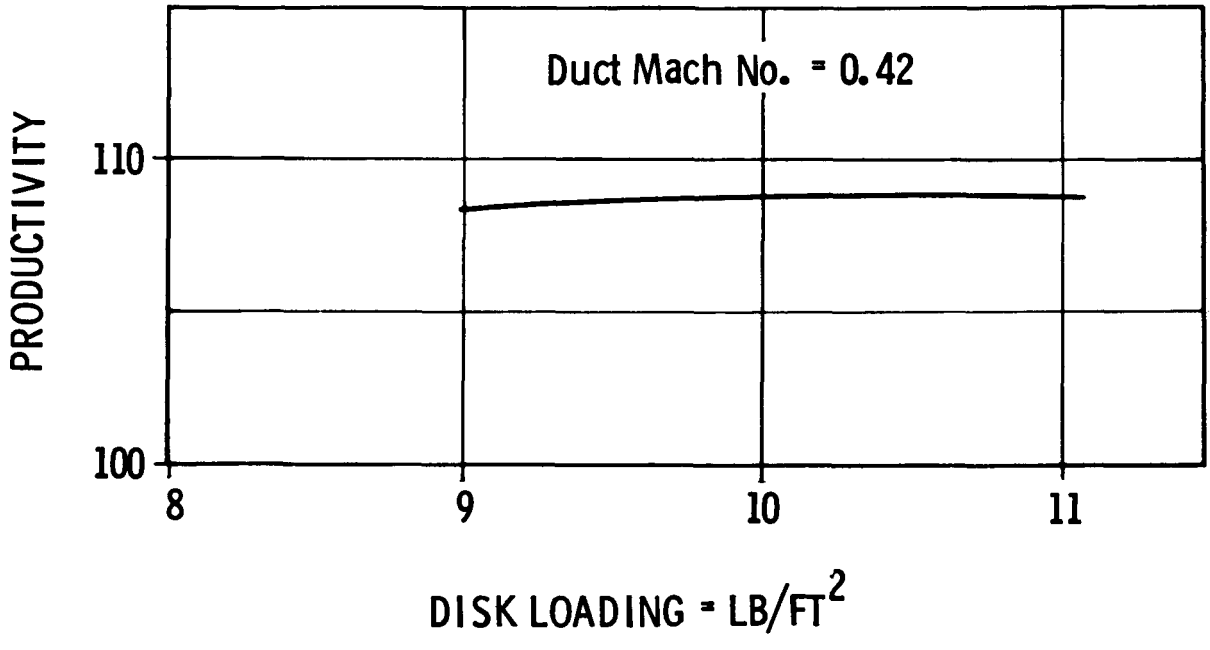

Figure 5. Warm Cycle - No Jet Flap - Effect of Disk Loading on Productivity

Effect of duct Mach Number (Chord).- Table 4 and Figure 6 show the effect of duct Mach Number on Productivity. The baseline parameters were:

a. Disk loading = 9.0 lb/ft^2
b. Gas flow split = 30% flap/70% nozzle
c. Flap length/radius = 0.275 (.7R - .975R)
d. Flap deflection = 40^o (hover), $20^o \pm 20^o \sin \Psi$ (cruise)
e. No. of blades = 3
f. Blade thickness ratio = .20
g. Blade tip speed, ft/sec = 700

TABLE 4

HOT CYCLE - EFFECT OF DUCT MACH NUMBER (CHORD)

Duct Mach Number	.306	.383	.428	.463
C - in.	44.0	40.3	38.9	37.8
R - ft.	63.0	63.0	63.0	63.0
σ	.0556	.0509	.0491	.0477
Disk Loading-lb/ft^2	9.02	9.00	9.02	8.95
% Engine Airflow-P_{air}	.461	.467	.477	.479
Payload - tons	30.14	30.17	30.19	29.80
Productivity	127.4	129.9	130.4	129.8
C_T/σ	.1724	.1880	.1953	.1994
$\alpha_{(1.0(270)}$Margin-deg	1.20	-.09	-.90	-1.36
W_g - lb	112116	111828	112206	111290
Fuel/Payload	.2081	.2128	.2198	.2257

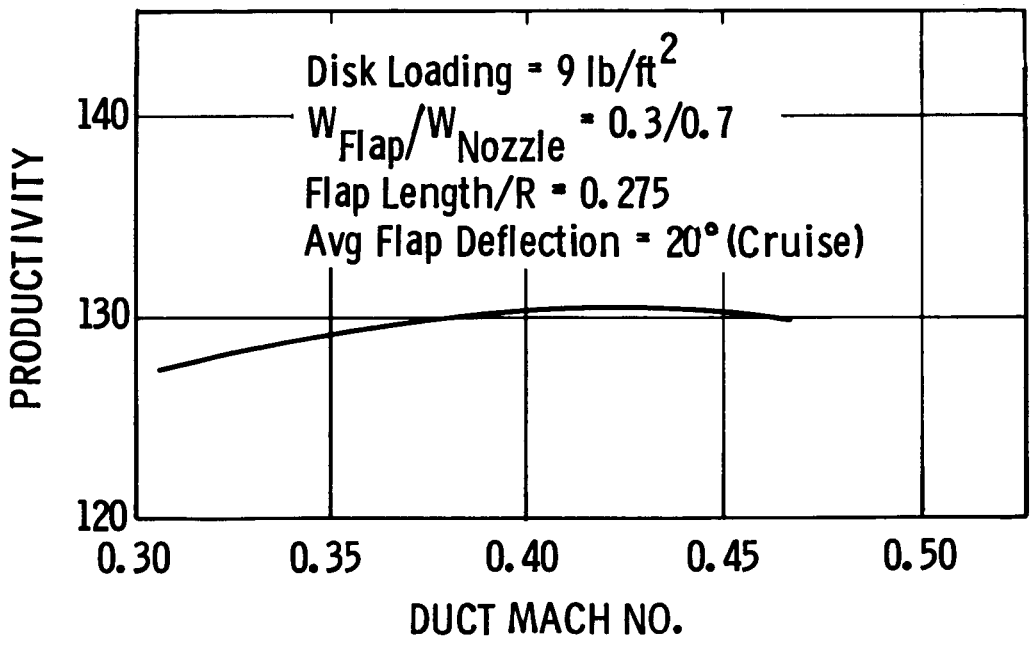

Figure 6. Hot Cycle Jet Flap - Effect of Duct Mach Number on Productivity

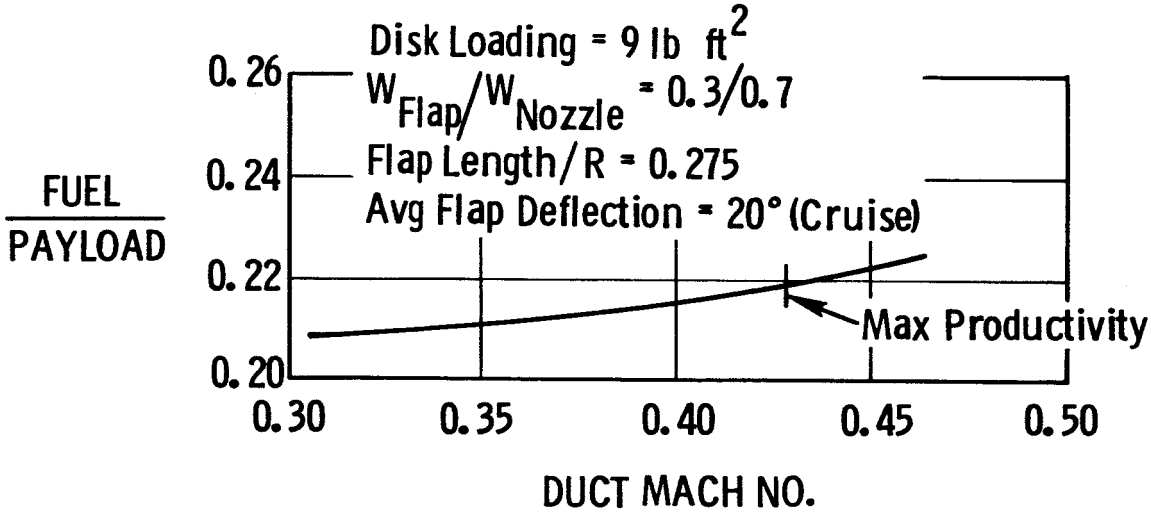

Figure 6a. Hot Cycle Jet Flap - Effect of Duct Mach Number on Fuel/ Payload Ratio

Figure 6 shows that in the Mach Number range from .306 to .463 the highest productivity (130.4) is obtained at a duct Mach Number = .428. Table 4 shows that C_T/σ for this configuration is .195, which is roughly 70% higher than that obtained for the reference Warm Cycle. At the same time, productivity is 130.4/108.8 or 20% higher. The blade tip angle of attack margin is -.9 degrees, which is lower than the allowable of -1.50 degrees. It is also seen that the highest duct Mach Number = .463 will allow a further increase of C_T/σ to .199, but only at the expense of a lower productivity and a tip angle closer to the limit value.

Effect of disk loading (radius).- Table 5 and Figure 7 show the effect of disk loading on Productivity. The baseline parameters were the same as for the duct Mach Number review above, except duct Mach Number was held essentially constant at .428 and disk loading was varied.

TABLE 5

HOT CYCLE - EFFECT OF DISK LOADING (RADIUS)

Disk Loading-lb/ft^2	7.05	8.07	9.02	10.06
R - ft	70.70	66.10	63.08	59.50
C - in	37.1	37.9	38.9	39.6
σ	.0418	.0456	.0491	.0529
Duct Mach Number	.423	.426	.428	.427
% Engine Airflow-P_{air}	.432	.452	.478	.494
Payload - tons	29.93	29.86	30.19	29.71
Productivity	129.7	130.1	130.4	129.0
C_T/σ	.1794	.1882	.1953	.2021
$\alpha_{(1.0)(270)}$Margin-deg	.93	.03	-.90	-1.92
W_g - lb	110499	110552	112206	111566
Fuel/Payload	.2046	.2112	.2198	.2320

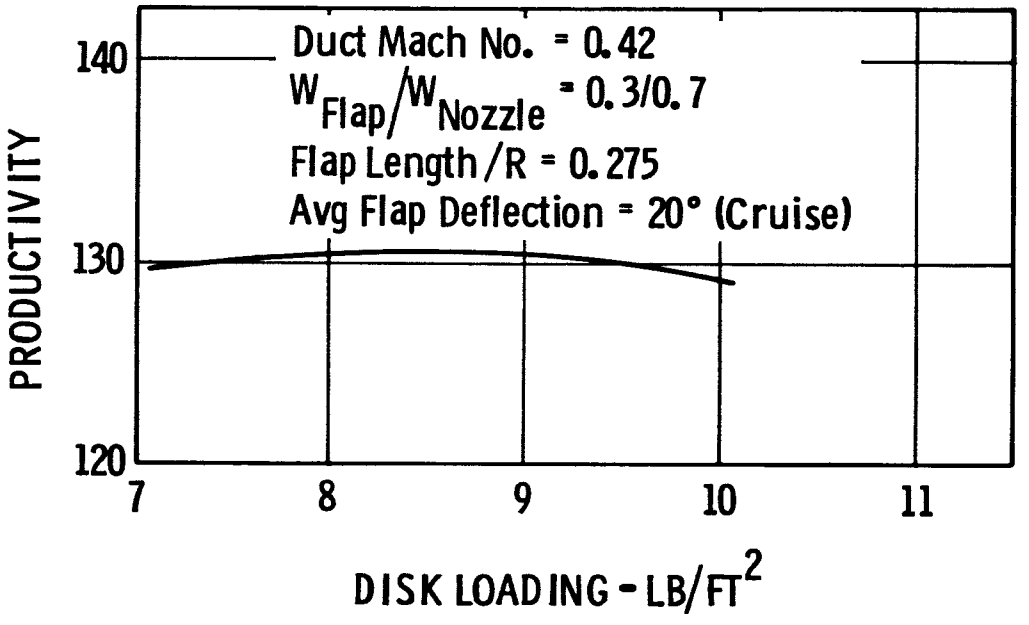

Figure 7. Hot Cycle Jet Flap - Effect of Disk Loading on Productivity

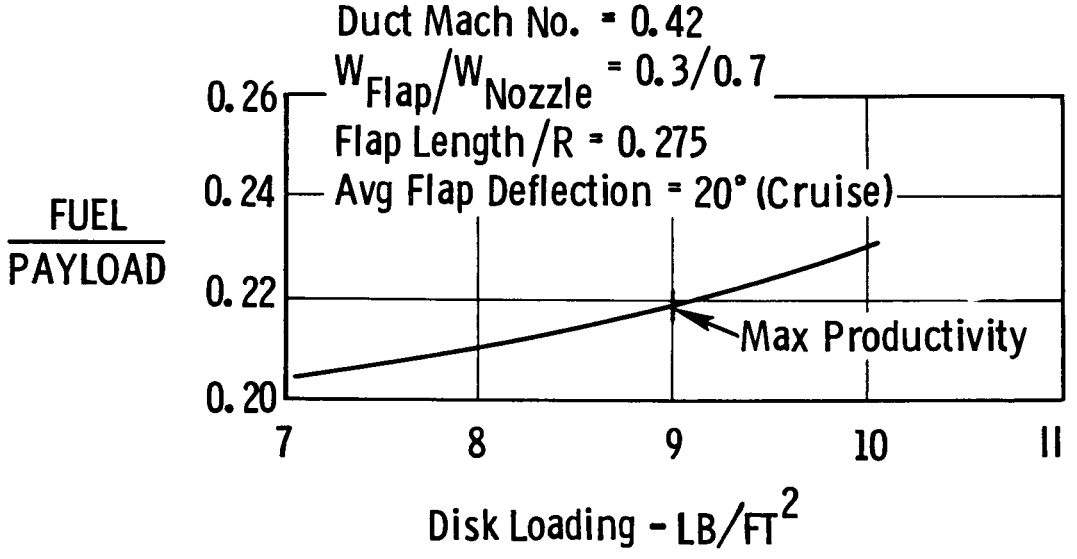

Figure 7a. Hot Cycle Jet Flap - Effect of Disk Loading on Fuel/Payload Ratio

Figure 7 shows that in the disk loading range from 7 to 10 pounds per square foot, the highest productivity is obtained at a disk loading of 9.0 pounds per square foot. Table 5 again shows that C_T/σ = .195, and productivity is 130.4, as noted above for Mach Number variation. It is also seen that a disk loading of 10 pounds per square foot would produce a C_T/σ = .202, but the blade tip angle of attack will exceed the allowable limit of -1.50 degrees margin.

Effect of gas split.- Table 6 shows the effect on productivity of gas split between the jet-flap and the tip nozzle. The baseline parameters are similar to those for duct Mach Number, except duct Mach Number of approximately .38 was used, and gas split to the flap and nozzle was varied.

TABLE 6

HOT CYCLE - EFFECT OF GAS SPLIT

Gas split, flap/nozzle	.3/.7	.35/.65	.4/.6	1.0/0
R - ft	62.96	63.36	63.60	64.50
C - in	40.5	40.3	40.7	46.9
σ	.0509	.0509	.0509	.0563
Duct Mach Number	.383	.383	.383	.377
Disk Loading-lb/ft^2	9.00	8.93	8.84	9.10
% Engine Airflow-P_{air}	.469	.475	.478	.627
Payload - tons	30.17	30.30	30.13	30.17
Productivity	129.9	129.7	128.7	117.4
C_T/σ	.1880	.1865	.1847	.1673
$\alpha_{(1.0)(270)}$Margin-deg	-.09	.72	1.50	7.97
W_g - lb	111828	112350	112110	118544
Fuel/Payload	.2128	.2127	.2144	.2590

Table 6 shows, in the range of gas split to the flap/nozzle varying from .3/.7 to 1.0/0, that a .3/.7 value gives the highest productivity (129.9). Any lower flow, such as 25% - 20% to the flap, will give essentially the same productivity, at the expense of more negative blade angles of attack. Therefore, the value

of gas split, flap/nozzle, = .3/.7 was used in the preceding two parameter studies. C_T/σ also decreases steadily with any increase in flow to the flap.

Effect of flap length/radius.- Table 7 shows the effect of jet-flap length/R on Productivity. The baseline parameters are similar to those for duct Mach Number, except that a Mach Number of .38, and a gas split of .35/.65 were used.

TABLE 7

HOT CYCLE - EFFECT OF FLAP LENGTH/RADIUS

Jet-flap length/R	.225	.275	.325
R - ft	63.30	63.40	63.28
C - in	40.5	40.5	40.5
σ	.0509	.0509	.0509
Duct Mach Number	.383	.383	.384
Disk Loading-lb/ft^2	8.92	8.93	8.92
% Engine Airflow-P_{air}	.473	.475	.474
Payload - tons	30.13	30.30	30.17
Productivity	129.3	129.7	129.4
C_T/σ	.1863	.1865	.1864
$\alpha_{(1.0)(270)}$ Margin-deg	.54	.72	.82
W_g - lb	111871	112350	111993
Fuel/Payload	.2131	.2127	.2133

Table 7 shows that in the range of jet-flap length/R from .225 - .325 that a flap length of .275 gave the highest productivity (129.7) by a slight margin. Further, (C_T/σ) is highest at a flap length/R = .275. Therefore, a flap length/R = .275 was used in the preceding three parameter studies.

Effect of flap deflection-cruise and hover.- Table 8 shows the effect on Productivity of jet-flap deflection in cruise. The baseline parameters were:

a. Disk loading = 8.1 lb/ft^2

b. Gas flow split = 30% flap, 70% nozzle

c. Duct Mach Number = .42

d. Flap length/radius = .275 (.7R - .975R)

e. No. of blades = 3

f. Blade thickness ratio = .20

g. Blade tip speed, ft/sec = 700

In Table 8, the hover flap deflection was arbitrarily fixed at the maximum value used in cruise.

TABLE 8

HOT CYCLE - EFFECT OF FLAP DEFLECTION (CRUISE)

Cruise flap deflection-degrees	15-15 sinΨ	20-20 sinΨ	25-25 sinΨ
Hover flap deflection-degrees	30	40	50
R - ft	66.10	66.10	66.50
C - in	37.9	37.9	38.1
σ	.0456	.0456	.0456
Duct Mach Number	.426	.426	.426
Disk Loading - lb/ft^2	8.12	8.07	7.98
% Engine Airflow - P_{air}	.453	.453	.458
Payload - tons	29.98	29.86	29.78
Productivity	130.2	130.1	129.1
C_T/σ	.1892	.1882	.1861
$\alpha_{(1.0)(270)}$ Margin-deg	.88	.03	-2.60
W_g - lb	111150	110552	110657
Fuel/Payload	.2144	.2112	.2134

Table 8 shows that, in the range of cruise flap deflection of 30^{o} to 50^{o} (maximum), highest relative productivity (130.2) is found at a flap deflection of 15^{o} - 15^{o} sinΨ. However, this productivity result is only very slightly better (130.2) than the value (130.1) obtained with 20^{o} - 20^{o} sinΨ deflection, which was used in the four preceding parameter studies. Therefore, it is concluded that the originally determined values of best duct Mach Number, disk loading, gas split, and flap length can be accepted based on the cruise flap deflection angle of 20^{o} - 20^{o} sinΨ with which they were determined. In addition, (C_T/σ) at 20^{o} - 20^{o} sinΨ is essentially the same as at 15^{o} - 15^{o} sinΨ.

Table 9 shows the effect on Productivity of jet-flap deflection in hover. The baseline parameters were the same as those for flap deflection in cruise, except that cruise flap deflection was held constant at 20^{o} - 20^{o} sinΨ.

TABLE 9

HOT CYCLE - EFFECT OF FLAP DEFLECTION (HOVER)

Hover flap deflection-degrees	30	40	50
Cruise flap deflection-degrees	20-20 sinΨ	20-20 sin Ψ	20-20 sinΨ
R - ft	66.1	66.1	66.5
C - in	37.9	37.9	38.3
σ	.0456	.0456	.0458
Duct Mach Number	.426	.426	.421
Disk Loading-lb/ft^2	8.12	8.07	7.99
% Engine Airflow-P_{air}	.453	.453	.458
Payload - tons	30.10	29.86	29.88
Productivity	130.8	130.1	129.4
C_T/σ	.1892	.1882	.1855
$\alpha_{(1.0)(270)}$ Margin-deg	-.09	.03	.31
W_g - lb	111150	110552	110820
Fuel/Payload	.2100	.2112	.2111

Table 9 shows that highest relative Productivity (130.8) was found at a hover flap deflection of 30^{o}, which is about 0.5% better than that (130.1) associated with a hover flap deflection of 40^{o}, the value used in the initial four hot cycle parameter studies. It is concluded that a hover flap deflection of 30^{o} is best, and that best values of duct Mach Number, gas split, and flap length/R determined on the basis of a cruise flap deflection of $20^{o} - 20^{o} \sin\Psi$ are acceptable. Adjusting for a disk loading of 9 pounds per square foot instead of 8 pounds per square foot, productivity for best hover flap angle becomes 131.0 (from Table 5 and Table 9).

This value of Productivity will be taken as the optimum for the Hot Cycle Heavy-Lift Helicopter. It is 131.0/108.8, or 21% higher than the reference Warm Cycle, no-jet-flap value. The associated C_T/σ based on Tables 5 and 9, is .196. Fuel/Payload is .22 (interpolated).

Effect of blade thickness ratio.- Table 10 shows the effect on Productivity of a change in the blade thickness ratio from a baseline value of .20 to .22. All other parameters are similar to those in item 1 (duct Mach Number), except the baseline disk loading was changed to 9 pounds per square foot.

TABLE 10

HOT CYCLE - EFFECT OF BLADE THICKNESS RATIO

Thickness Ratio	.20	.22
R - ft	62.96	62.80
C - in	40.3	38.4
σ	.0509	.0487
Duct Mach Number	.383	.380
Disk Loading - lb/ft^2	9.00	8.99
% Engine Airflow-P_{air}	.469	.466
Payload - tons	30.17	29.95
Productivitv	129.9	130.7
C_T/σ	.1880	.1963
$\alpha_{(1.0)(270)}$ Margin-deg	-.09	-1.03
W_g - lb	111828	111129
Fuel/Payload	.2128	.2177

Table 10 shows that the added 10% thickness produces about a 0.6% increase in Productivity, based on aerodynamic and propulsion considerations only. However, the added thickness will raise the blade natural frequency, possibly leading to excessive stresses. For this reason, and because of the small effect of increased thickness on productivity, thickness ratio was retained at .20.

Effect of change of blade camber.- A review was made of the angle of attack distribution down the blade, and it became clear that, although the blade in the region of the jet-flap was heavily loaded, the blade inboard of the jet-flap was not carrying as much load as seemed reasonable. Therefore, a change in blade camber inboard of the jet-flap was simulated by imposing an equivalent increase of blade pitch angle. Both $\theta_{CAM} = 3^{o}$ and $\theta_{CAM} = 4^{o}$ were tried, and the $\theta_{CAM} = 4^{o}$ value gave a 4% higher productivity. Therefore, this value was used throughout the entire study.

Effect of flap pitch distribution.- The jet-flap used here was assumed to be broken into four segments of equal length, each having the same pitch setting at the same time. As discussed in Appendix A, the computer program was assembled with the capability of varying the pitch of the individual flap segments. This feature was not used in this initial study, and could be included in any future study of the jet-flap helicopter.

Warm Cycle Propulsion System

A brief set of Warm Cycle cases with a jet-flap was run to establish possible performance with this type of propulsion system. The results are shown in Table 11 and Figure 8. As mentioned earlier, preliminary calculations were made which established that highest productivity can be obtained with the Hot Cycle. The Hot Cycle was used to find the sensitivity of the several jet-flap parameters discussed above. Using those studies as a guide, the baseline parameters for the Warm Cycle study were as follows:

a. Disk loading = 10 lb/ft^2
b. Gas flow split = 30% flap/70% nozzle
c. Flap length/radius = .275 (.7R-.975R)
d. No. of blades = 3
e. Blade thickness ratio = .20
f. Blade tip speed, ft/sec = 700
g. Flap deflection angle (hover) 40^{o}

Flap deflection angle in cruise was $10^{o} - 10^{o} \sin\Psi$, which is lower than used previously. This results from the fact that the internal thermodynamics of the Warm Cycle requires a solidity that is higher than that of the Hot Cycle. As a result, less help is needed from the jet-flap to obtain equilibrium about the flapping hinge. Consequently, less flap deflection is required to obtain the limiting C_T/σ.

TABLE 11

WARM CYCLE - EFFECT OF DUCT MACH NUMBER (CHORD)

Duct Mach Number	.408	.453	.498
C - in	54.4	52.8	51.4
R - ft	60.60	60.60	60.75
σ	.0715	.0693	.0582
Disk Loading - lb/ft^2	10.04	10.09	10.05
% Engine Airflow - P_{air}	.449	.458	.466
Payload - tons	29.87	30.04	29.97
Productivity	118.2	119.2	119.2
C_T/σ	.1492	.1547	.1587
$\alpha_{(1.0)(270)}$ Margin-deg	3.36	2.94	2.64
W_g - lb	115486	116078	116198
Fuel/Payload	.2124	.2170	.2231

Figure 8 shows that, in the Mach Number range from .4 to .5, highest productivity (119.5) is obtained at a duct Mach Number =.475. Interpolation in Table 11 shows that C_T/σ for this configuration is .157, which is roughly 37% higher than that obtained for the reference Warm Cycle - no-jet-flap configuration. Productivity is 119.5/108.8 or 10% higher with the jet-flap. Interpolated fuel/payload is .22.

A few Warm Cycle jet-flap cases were run with two blades, at a disk loading of 10 pounds per square foot. Productivity was found to be 129.4 at a duct Mach Number = .450 with C_T/σ = .1904. (Fuel/Payload was .2138) Obviously, going to two blades will permit a lower solidity and give higher performance.

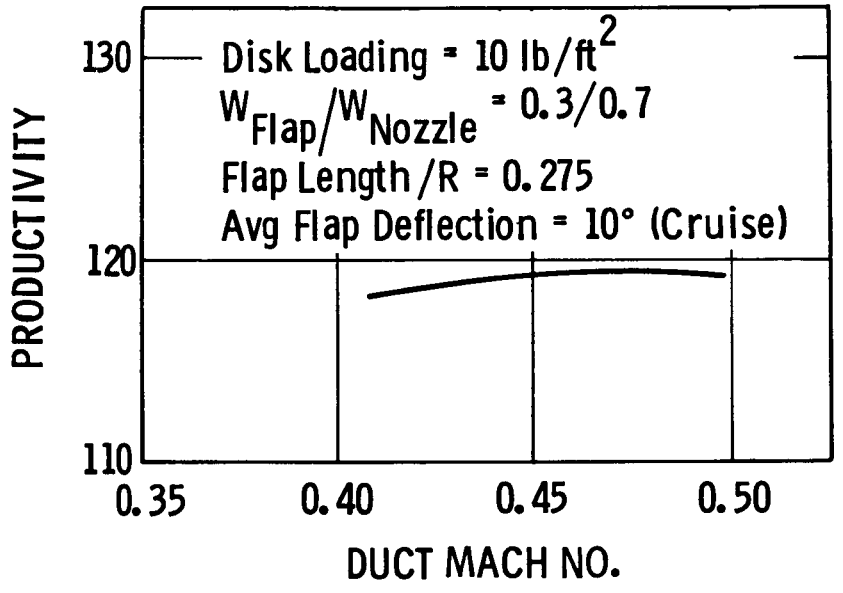

Figure 8. Warm Cycle Jet Flap - Effect of Duct Mach Number on Productivity

This Warm Cycle performance with two blades approaches that of the Hot Cycle. However, two-blade rotors introduce dynamic problems not present with 3- or 4- bladed rotors. Consequently, the Warm Cycle jet-flap case will be discussed relative to 3 blades.

Cold Cycle Propulsion System

Calculations which were made of the performance of the Cold Cycle propulsion system showed that although the highly compressed air permitted an aerodynamically-limited, lightweight, low solidity rotor, the added engine weight and fuel weight associated with this type of propulsion resulted in limiting the Productivity. The baseline parameters were the same as for the Warm Cycle with jet-flap, except jet-flap deflection in cruise was returned to $20^{o} - 20^{o} \sin\Psi$. Results are as follows:

TABLE 12

COLD CYCLE

Duct Mach Number	.260
C - in	41.0
R - ft	61.60
σ	.053
Disk Loading - lb/ft^2	10.17
% Engine Airflow - P_{air}	.601
Payload - tons	30.34
Productivity	120.6
C_T/σ	.2039
$\alpha_{(1.0)(270)}$ Margin-deg	-1.47
W_f - lb	120855
Fuel/Payload	.2658

Table 12 shows that the Cold Cycle is aerodynamically limited, with no thermodynamic constraints. The duct Mach Number of .260 is the lowest of any examined, the C_T/σ = .204 is the highest, and the blade tip angle is essentially at the limit margin of -1.50 degrees. The productivity 120.6 is lower than that of the Hot Cycle systems, and is slightly higher than that of the Warm Cycle.

Comparison of Propulsion Systems

The following table presents the best interpolated configuration of the several propulsion systems, in order to provide a rapid evaluation of the utility of the jet-flap.

TABLE 13

COMPARISON OF PROPULSION SYSTEMS

Propulsion Type	Warm Cycle	Hot Cycle	Warm Cycle	Cold Cycle
Jet-Flap	No	Yes	Yes	Yes
Productivity	108.8	131.0	119.5	120.6
C_T/σ	.115	.196	.157	.204
Duct Mach Number	.42	.43	.47	.26
Disk Loading-lb/ft^2	10.1	9.0	10.1	10.2
Fuel/Payload	.23	.22	.22	.27

Table 13 shows that the Hot Cycle propulsion system offers the best jet-flap Productivity, followed by the Cold Cycle, and lastly by the Warm Cycle, compared to the Warm Cycle, no-jet-flap. In addition, for reference purposes, the ratio of fuel/payload is given. It is seen that the Hot Cycle and Warm Cycle jet-flap configurations have essentially the same ratio of fuel/payload as the reference Warm Cycle - no-jet-flap helicopter. Apparently, the reduction in profile power associated with the lower solidity of the jet-flap rotor is enough to overcome the relative inefficiency of the jet-flap, which exhausts the gas only part way to the blade tip, in a downward direction, thereby raising the specific fuel consumption.

The Cold Cycle rotor, on the other hand, experiences an 18% increase of the fuel/payload ratio.

RESULTS OF THE HIGH SPEED MANEUVERABILITY JET-FLAP STUDY

The results of the 200 knots, 2g jet-flap study indicate that the desired maneuverability can be obtained with a rotor design very consistent with NASA tests of a similar jet-flap rotor. The solidity required for the design condition permitted the use of the Warm Cycle propulsion system because duct size was aerodynamically, not thermodynamically, limited. The determination of the best combination of jet-flap parameters is as follows:

Effect of Gas Split

A set of exploratory calculations were run using only the modified performance program to define the flap parameters most likely to produce the desired rotor performance. An initial gas split of 0.3 flap/0.7 nozzle, which was the preferred Heavy-Lift split, produced a retreating blade tip angle of attack of almost 20^{o} past the allowable value. Splits of .5 flap/.5 nozzle and 0.75 flap/0.25 nozzle also resulted in excessive angle of attack, and a split of 1.0 flap/0.0 nozzle was required for satisfactory operation.

Effect of Jet-Flap Deflection

Simultaneously with variation of the gas split, jet-flap deflection angles were varied in hover and cruise. It was found that, to obtain satisfactory blade tip angles of attack, the flap deflection required was that which produced maximum lift coefficient for a given jet momentum coefficient. As discussed in Appendix C, the Jet-Flap Aerodynamic Characteristics section, this corresponds to a deflection of 40^{o} in hover, and $20^{o} - 20^{o}$ sin Ψ in cruise.

Effect of Flap Length/Radius

Table 14 shows the effect of jet-flap length/R on Productivity. The baseline parameters were:

a. Disk loading = 10.3 lb/ft^2
b. Gas flow split = 100% flap/0% nozzle
c. Duct Mach Number = .31
d. Flap deflection = 40^{o} (hover), 20^{o}-20^{o} sinΨ (cruise)
e. No. of blades = 4
f. Blade tip speed = 650 ft/sec
g. Cruise speed = 200 knots

TABLE 14

HIGH SPEED - EFFECT OF FLAP LENGTH/RADIUS

Jet-Flap Length/R	.375	.275	.175
R - ft	27.00	27.00	27.00
C - in	33.8	33.8	33.8
σ	.133	.133	.133
Disk Loading - lb/ft^2	10.23	10.37	10.08
% Engine Airflow - P_{air}	.136	.136	.136
Payload - tons	3.02	3.17	2.94
Productivity	85.8	90.0	84.2
C_T/σ (2g)	.1638	.1659	.1614
$\alpha_{(1.0)(270)}$ Margin-deg	.13	-.77	-2.05
W_g - lb	23509	23814	23164
Fuel/Payload	.6566	.6190	.6562

Table 14 shows that a flap length/R of .275R gives the highest productivity and highest C_T/σ, and that value was therefore used for further optimization.

Effect of Disk Loading - (Radius)

Table 15 shows the effect of disk loading on productivity. The baseline parameters were the same as for the study of flap length/radius.

TABLE 15

HIGH SPEED - EFFECT OF DISK LOADING (RADIUS)

Disk Loading lb/ft^2	9.05	10.37	11.01
R - ft	29.00	27.00	26.00
C - in	33.3	33.80	34.0
σ	.122	.133	.139
Duct Mach Number	.308	.307	.305
% Engine Airflow-P_{air}	.133	.136	.137
Payload - tons	3.12	3.17	3.10
Productivity	87.2	90.0	89.2
C_T/σ (2g)	.1580	.1659	.1687
$\alpha_{(1.0)(270)}$ Margin-deg	.24	-.77	-1.02
W_g - lb	23997	23814	23459
Fuel/Payload	.6448	.6190	.6214

Table 15 shows that highest productivity is obtained with a disk loading of 10.4 pounds per square foot.

Effect of Duct Mach Number (Chord)

Table 16 shows the effect of duct Number on productivity. The baseline parameters (except Mach Number) were the same as for the flap length/R review above.

TABLE 16

HIGH SPEED - EFFECT OF DUCT MACH NUMBER (CHORD)

Duct Mach Number	.307	.336	.367
C - in	33.8	32.8	31.8
R - ft	27.00	27.00	27.00
σ	.133	.129	.125
Disk Loading - lb/ft^2	10.37	10.3	10.25
% Engine Airflow-P_{air}	.136	.138	.141
Payload - tons	3.17	3.16	3.14
Productivity	90.0	90.3	90.1
C_T/σ (2g)	.1659	.1703	.1746
$\alpha_{(1.0)(270)}$ Margin-deg	-.77	-1.31	-1.87
W_g - lb	23814	23668	23552
Fuel/Payload	.6190	.6184	.6227

Table 16 shows that within the Mach Number range examined, the effect on productivity is practically nil, and a duct Mach Number of .34 gives the highest productivity (90.3). The corresponding C_T/σ is .170. This configuration is selected as the preferred high speed maneuverable (200 knot, 2g) helicopter.

Comparison with NASA Work

An interesting comparison of the high speed rotor lift capability using the jet-flap is shown in Figure 9. This figure is taken from Reference 8, and shows the calculated lift capability of the U.S.Army/Dorand Jet-Flap rotor. (Some test points are included, but mechanical pitch limits prevented reaching full rotor capability).

Spotted on the band labeled "calculated NASA TN D-3028" is the calculated point taken from the preceding section of this report. This point falls into the band calculated by NASA for lift of a

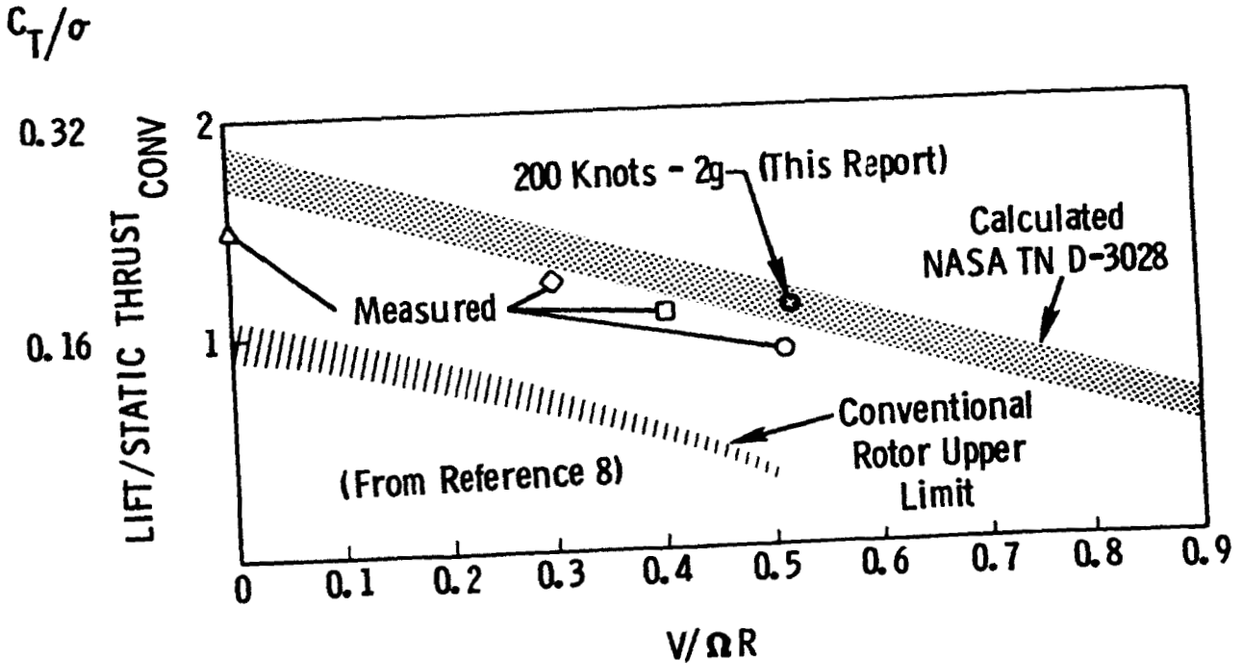

Figure 9. Jet-Flap Rotor Capability

representative jet-flap rotor, and this shows consistency between the two studies.

An added aspect of this comparison is shown on Figure 10. This figure, also taken from Reference 8, shows the rotor lift force vs rotor propulsive force, using the appropriate parasite area value. It is seen that the calculated C_{L_R}/σ and C_{X_R}/σ values are quite consistent with the test values from Reference 8.

A preliminary study was also made of the configuration of a conventional no-jet-flap rotor able to fly at 200 knots at 2g. Using the charts of Reference 9, and increasing the Upper Stall Limit by $\Delta\ (C_T/\sigma) = .04$ based on tests reported in Reference 10, the allowable C_T/σ is .083 at $\mu = .52$ for the conventional rotor, leading to a solidity of .245, which is twice that needed by the jet-flap rotor. Therefore, it is concluded that a pure helicopter with a conventional rotor will require a rotor with double the solidity of a jet-flap rotor when performaing the 200 knot, 2g mission.

EFFECT OF REDUCED POWER AND AUTOROTATION

High lift coefficients are developed on the rotor blades through the blowing of a gas jet over a deflected mechanical flap. If the momentum in the air jet should be reduced, the increased lift coefficient would be reduced and blade stall would occur. Therefore, partial power descents and engine failure were studied to find methods of alleviating this problem.

Heavy-Lift Helicopter

In the case of partial power descent, the optimum configuration has 1 to 1.5° margin below the limit angle of attack in level flight, and the angle of attack will reduce slightly in descent. Therefore, with less blowing, it might be possible to descend at constant airspeed without blade stall. If further work shows that stall does occur, it might be necessary to reduce airspeed before entering descent. As an alternate, since the heavy-lift helicopter applies only 30% of the gas flow to the jet-flap, a system of variable area nozzles could be used to reduce the fraction of flow to the tip nozzles at part power and to increase the flow to the jet-flap.

The heavy-lift configuration will have three engines. Therefore, in case of failure of a single engine, cross-over ducting will be provided to maintain the proper gas flow in the jet-flap area. In the case of complete power failure, it will be possible to

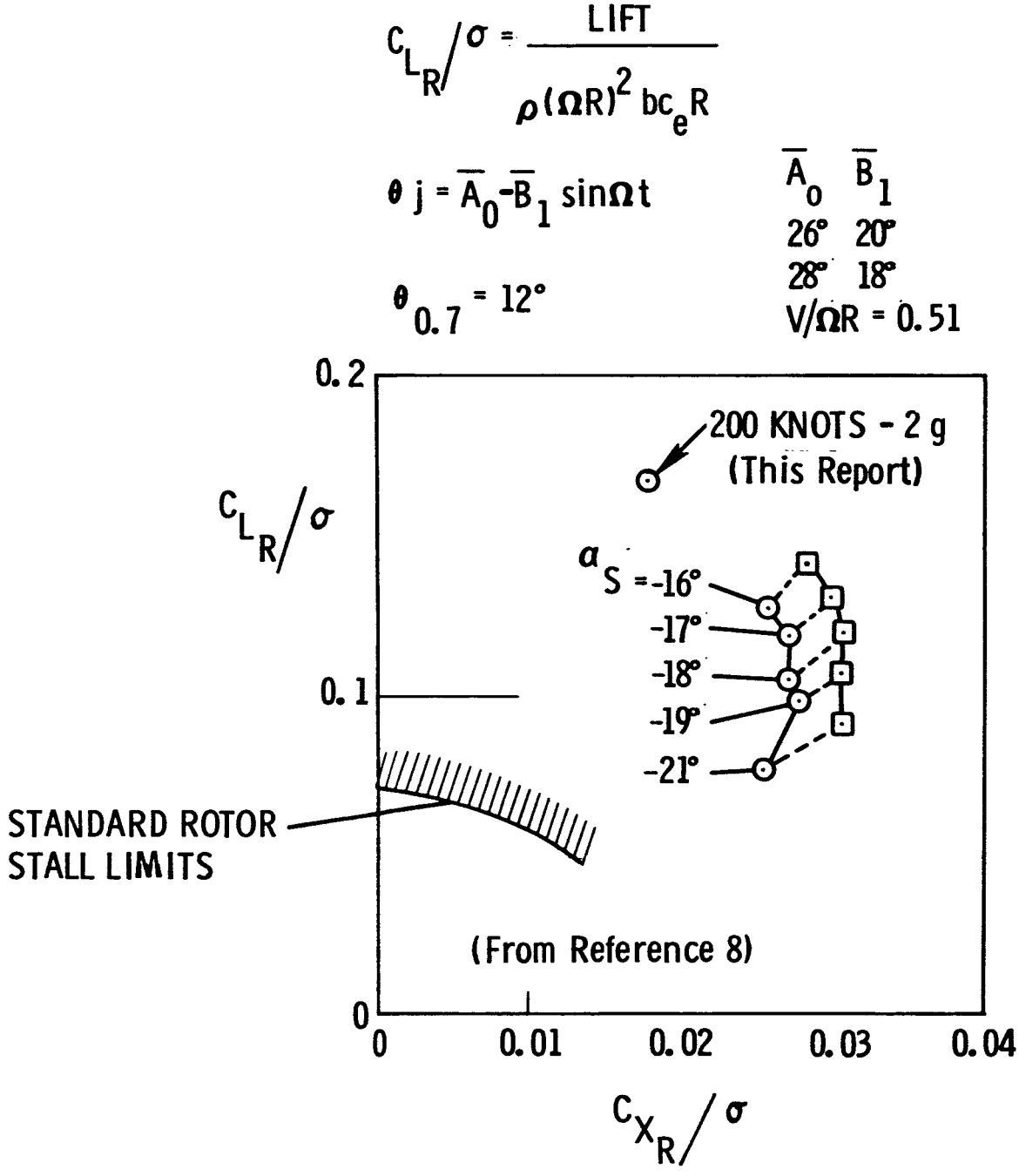

Figure 10. Jet-Flap Rotor Force Capability

autorotate at increased tip speed (122% of power-on tip speed) without encountering blade stall.

High Speed Maneuverable Helicopter

The 200 knot helicopter was designed to perform a 2g turn in level flight. For this maneuver all the gas is diverted to the jet-flap section. It will be impossible to reduce torque for a descent and still perform a 2g maneuver, due to the reduction of momentum in the jet-flap area. As the 1g C_T/σ is not excessive (.085), level flight and descent are not a problem.

In case of complete engine failure at 200 knots at 1g, the pilot will have to decrease the forward speed to about 100 knots, in order to autorotate.

PRELIMINARY ESTIMATES OF JET-FLAP SIZE

The calculations discussed above have led to the sizing of the optimum helicopters for the Heavy-Lift mission and the 200 knot, 2g mission, using the best combination of jet-flap deflection, flap length, and gas split. The effect on blade aerodynamic characteristics of the jet-flap used in this study is given in Appendix C, wherein data is presented for blowing over the upper surface of a 12.5% chord flap attached to an NACA 0018 airfoil.

Because of the scarcity of data, mentioned earlier, it was assumed in this study that the same lift-augmentation results would apply to airfoils of 15% and 20% thickness ratios that have 12.5% chord flaps with upper surface blowing. It is then possible to find the proportions of jet-flap nozzle height and flap thickness, thus permitting a designer to proportion structure and hinge mechanism. In addition, it is possible to observe that the required nozzle height/flap thickness is of acceptable proportion, as seen in Table 17.

For power-on flight the nozzle size shown is not expected to cause any difficulties; for power-off flight, some nozzle base drag would be introduced, particularly for the 200 knot, 2g configuration.

TABLE 17

JET-FLAP NOZZLE HEIGHT/FLAP THICKNESS

Helicopter Type	Blade Radius ft	Flap Length ft	Blade Chord in	Flap Chord in	Airfoil Thickness Ratio
Heavy-Lift	63.0	17.3	38.9	4.9	.20
200 knots, 2g	27.0	7.4	31.8	4.0	.15

	Flap Thickness at Hinge - in	Nozzle Height in	Nozzle Height/ Flap Thickness
Heavy-Lift	2.26	.146	.07
200 knots, 2g	1.39	.484	.35

CONCLUSIONS

Heavy-Lift Helicopter Mission

The increase in maximum airfoil lift coefficient achieved by the jet-flap permits a reduction of rotor solidity to approximately 59% of a non-jet-flap rotor.

As a result of the saving in rotor solidity, and hence in rotor weight, the jet-flap configurations had a 21% higher productivity than a non-jet-flap configuration.

Of the three propulsion systems studied utilizing a jet-flap (Hot Cycle, Warm Cycle, Cold Cycle) the Hot Cycle gave the largest increase in productivity.

Fuel/payload ratios with the Hot Cycle and Warm Cycle jet-flap propulsion systems are the same as for the reference Warm Cycle no-jet-flap Warm Cycle; the fuel/payload ratio for the Cold Cycle is 18% higher.

The highest productivity is obtained with the following rotor and jet-flap parameters:

Duct Mach Number	.43
Disk Loading	9 lb/ft^2
Gas Split	30% flap/70% tip nozzle
Flap Length/Radius	.275
Jet-Flap Deflection-Hover:	30^o
-Cruise:	$15^o - 15^o \sin\Psi$

200 Knot 2g Mission

The 200 knot 2g mission is performed best with a Warm Cycle propulsion system. The jet-flap permits designing for a rotor blade loading coefficient $C_T/\sigma = .170$ at 2g without encountering blade stall. A conventional rotor will allow a C_T/σ of only .083 at 200 knots. Thus, the jet-flap rotor permits a 200 knot 2g maneuver without suffering the penalty of an unreasonable rotor solidity that would be required by a non-jet-flap rotor.

The rotor and jet-flap parameters for the preferred configuration are:

Duct Mach Number		.34
Disk Loading		10.4 lb/ft^2
Gas Split		100% flap/0% tip nozzle
Flap Length/Radius		.275
Jet-Flap Deflection	- Hover:	40^o
	- Cruise:	$20^o - 20^o \sin\Psi$

Airfoil Data

There is only partial test data on the drag of jet-flap airfoils in the stall region, as affected by momentum coefficient.

RECOMMENDATIONS

Data for jet-flap airfoils should be obtained on lift coefficient and drag coefficient vs momentum coefficient for angles of attack several degrees past stall.

The influence of Mach Number on jet-flap airfoil characteristics should be determined.

Jet-flap nozzle pressure ratios up to 4.5 should be studied.

A design study should be performed of the high speed maneuverability mission to determine the relative productivity of the pure helicopter with a jet-flap rotor, the pure helicopter with a very high solidity rotor, and other configurations of interest such as the compound helicopter.

C2

APPENDIX A

ROTOR PERFORMANCE CALCULATION

Introduction

The rotor performance subroutine consists of two parts. The first part is used to compute the rotor flapping angles and is based on the equations presented in Reference 3. The second part uses the flapping values obtained in the first part and computes the aerodynamic characteristics of the rotor based on equations from Reference 4.

In the present jet-flap study nine radial stations are assumed on the blade portion inboard of the jet-flap and five stations on the jet-flap. Eighteen azimuth positions are used. In the following discussion, those terms which have been added to handle the jet-flap are underlined.

Angle of Attack and Section Characteristics for Unflapped Blade

At each station and azimuth, the following equations are used to compute local angle of attack and Mach Number. All terms are with respect to the rotor shaft axis.

$$U_{P_s} = \lambda_s \cos\beta - \left(x - \frac{e}{R}\right)\dot{\overline{\beta}} - \mu_s \sin\beta \cos\Psi \qquad \text{(A-1)}$$

$$U_{T_s} = \frac{e}{R} + \left(x - \frac{e}{R}\right)\cos\beta + \mu_s \sin\Psi \qquad \text{(A-2)}$$

$$\phi = \tan^{-1}\left(\frac{U_{P_s}}{U_{T_s}}\right) \qquad \text{(A-3)}$$

$$U = \sqrt{U_{P_s}^2 + U_{T_s}^2} \qquad \text{(A-4)}$$

The local angle of attack is

$$\alpha_{r_p} = \theta_o + \theta_1 x - A_1 \cos\Psi - B_1 \sin\Psi + \phi + \underline{\theta_{CAM}} \qquad \text{(A-5)}$$

The local Mach Number is

$$M_X = \frac{U\ \Omega R}{a} \qquad \text{(A-6)}$$

By using the section angle of attack and Mach Number, C_ℓ and C_d for the basic rotor blade section exclusive of the jet-flap are obtained from tables of two dimensional airfoil data. (Reference 11)

Jet-Flap Momentum and Lift and Drag Coefficients

At each station on the jet-flap, mass flow and relative gas ejection velocity are computed during the rotor power available calculation discussed in Appendix B. Momentum coefficient is then computed at each station using the following equation:

$$C_j = \frac{2m\ V_j b}{\rho U^2 (\Omega R)^2 \sigma \pi R} \qquad \text{(A-7)}$$

The following equations are used to determined the C_ℓ and C_d contributed by the jet-flap:

$$C_{\ell_j} = C_j \sin(\alpha + \delta) + S_\ell\ C_j \sin(\alpha + \delta) \qquad \text{(A-8)}$$

$$C_{d_{o_j}} = -C_j \cos(\alpha + \delta) - S_d\ 1 - \cos(\alpha + \delta) \qquad \text{(A-9)}$$

The mechanical flap $C_{d_{MF}}$ is simply:

$$C_{d_{MF}} = \left(\frac{\partial C_{d_o}}{\partial \delta}\right)_{MF} \cdot \delta \qquad \text{(A-10)}$$

The expressions for total C_ℓ and C_d on the jet-flap portion are:

$$C_{\ell_j}' = C_{\ell_o} + \underline{C_j \sin(\alpha + \delta)} + \underline{S_\ell\ C_j \sin(\alpha + \delta)} \qquad \text{(A-11)}$$

$$C_{d_{o_j}}' = C_{d_o} - C_j \cos(\alpha + \delta) - S_d \left[1 - \cos(\alpha + \delta)\right] \Big/ \left[\left(\frac{\partial C_{d_o}}{\partial \delta}\right)_{MF} \cdot \delta\right] \tag{A-12}$$

Blade Flapping Characteristics

The procedure used to obtain the blade flapping characteristics is based on the fact that no moments may be transmitted through the blade flapping hinge. That is, the sum of all moments about the flapping hinge at any rotor azimuth position is zero.

$$M_T - M_C - M_I - M_W = 0 \tag{A-13}$$

The aerodynamic moment is given by

$$M_T = \frac{1}{2} I_h \Omega^2 \gamma' \Big[\int_{x_c}^{x_f} \left(x - \frac{e}{R}\right) U \left(C_\ell U_T + C_{d_o} U_P\right) dx + \int_{x_f}^{x_N} \left(x - \frac{e}{R}\right) U \left(C_{\ell_j}' U_T + C_{d_{o_j}}' U_P\right) dx - \int_{B}^{x_N} \left(x - \frac{e}{R}\right) U C_{\ell_j}' U_T \, dx + \frac{2}{\sigma} C_{Q_{NOZ}}' \sin\theta_N \tag{A-14}$$

The centrifugal force moment is

$$M_C = \Omega^2 \sin\beta \left(I_h \cos\beta + \frac{e}{g} M_W'\right) \tag{A-15}$$

The blade inertia moment is

$$M_I = \ddot{\beta} I_h$$

Expressing β in terms of Ψ

$$\ddot{\beta} = \Omega^2 \bar{\bar{\beta}} \tag{A-16}$$

$$M_I = \Omega^2 \bar{\bar{\beta}} I_h$$

The weight moment is given by

$$M_W = M'_W \cos \beta \qquad \text{(A-17)}$$

Substituting A-14, A-15, A-16 and A-17 into equation A-13 results in a differential equation in which

$$\dot{\beta} = f(\beta, \bar{\beta}) \qquad \text{(A-18)}$$

Initial values of β and $\bar{\beta}$ are assumed for the zero azimuth position and equation A-18 is solved for β. Using numerical integration, β and $\bar{\beta}$ are predicted for the next azimuth position. When the calculation has been completed for a full rotor revolution, the final β is compared with the initial β. If they agree within a specified tolerance, the calculation is complete. If not, the iteration is repeated, starting with the final value of β.

Rotor Coriolis Torque

Acceleration of the gas up to the local rotational speed of the rotor determines the Coriolis torque of the rotor. This quantity is influenced by how far along the rotor a particular quantity of gas travels before it is exhausted, as well as the amount of the gas. To determine this value, a numerical integration is performed which assumes the rotor to be broken up sequentially into an inboard section, four variable but equal-length jet-flap segments, and the tip nozzle. The proportion of the total flow exiting through a flap section j is an input variable K_j. The Coriolis torque coefficient is then determined as a function of gas flow (or engine power level):

$$C_{Q_{Coriolis}} = \frac{\frac{b W_g}{A \rho \Omega R g}\left[X_1^2 + \sum_{i=2}^{5}\left(X_i^2 - X_{i-1}^2\right)\left(1 - \sum_{j=1}^{i} K_j\right)\right]}{\text{Rotor Driving Torque}} \qquad \text{(A-19)}$$

The torque driving the rotor is made up of two parts, that due to the gas exhausting from the jet-flap and that due to the rest of the gas exhausting from the tip nozzle.

The jet-flap driving torque is associated with the $C_{D_{o_j}}$ term as "negative" drag in the drag coefficient equation A-9 given earlier. This "negative" drag coefficient is introduced into the

total drag coefficient $C_{D_{o_j}}'$ (A-12) which is converted into a torque coefficient in the next section in the equation for $C_{Q_{jf}}(\Psi)$ (A-30).

The tip nozzle driving torque is determined directly by the gases exhausting at the nozzle, as given in the following equation

$$C_{Q\ Nozzle}' = - \frac{W_g K_5 V_5 b}{gA\rho(\Omega R)^2} \qquad \text{(A-20)}$$

This term is converted to $C_{Q_{Noz}}(\Psi)$ in the next section (Equation A-32). Finally, both $C_{Q_{jf}}(\Psi)$ and $C_{Q_{Noz}}(\Psi)$ are combined in the equation A-23, which balances all accelerating and decelerating torques on the rotor.

Rotor Performance Equations

The rotor performance parameters are then computed using the following equations based on the final flapping angles obtained earlier. These equations formulate rotor thrust, torque, and horizontal force. They include the previously determined values of flapping angles, Coriolis torque, and jet-flap and tip nozzle driving torque. All of these equations are solved simultaneously by iteration, arriving at an engine power level that not only provides the power required to produce the required thrust and propulsive force, but also generates the proper jet-flap exhaust velocity to make the jet-flap operate at the required high lift coefficients.

Blade pitch at the tip nozzle is

$$\theta_N = \theta_o + \theta_1 + i_{Noz} - A_1 \cos\Psi - B_1 \sin\Psi + \theta_{cam} \qquad \text{(A-21)}$$

$$C_T = \frac{1}{n}\sum_{\psi=1}^{n}\left[C_{T,\ell} + C_{T,0} + \underline{\Delta C_{T\,NOZ}} \right] \qquad \text{(A-22)}$$

$$C_Q = \frac{1}{n}\sum_{\psi=1}^{n}\left[C_{Q,d} - C_{Q,a} + \underline{C_{Q_{Jf}}} + \underline{C_{Q_{mf}}} + \underline{C_{Q_{NOZ}}} \right] + \underline{C_{Q\,COR}} \qquad \text{(A-23)}$$

$$C_H = \frac{1}{n}\sum_{\psi=1}^{n}\left[C_{H,i} + C_{H,0} + \underline{\Delta C_{H_{NOZ}}} \right] \qquad \text{(A-24)}$$

for each azimuth, $\psi = 1, n$

$$C_{T,\ell}(\psi) = \int_{X_c}^{X_f} \tfrac{1}{2}\sigma_x u^2 C_\ell \cos\phi\, dx + \underline{\int_{X_f}^{B} \tfrac{1}{2}\sigma_x u^2 C'_{\ell_j} \cos\psi\, dx} \qquad \text{(A-25)}$$

$$C_{T,0}(\psi) = \int_{X_c}^{X_f} \tfrac{1}{2}\sigma_x u^2 C_{d_0} \sin\phi\, dx + \underline{\int_{X_f}^{X_N} \tfrac{1}{2}\sigma_x u^2 C'_{d_{0j}} \sin\phi\, dx} \qquad \text{(A-26)}$$

$$\Delta C_{T\,NOZ}(\psi) = \underline{-C'_{Q_{NOZ}} \sin\Theta_N} \qquad \text{(A-27)}$$

$$C_{Q,d}(\psi) = \int_{X_c}^{X_f} \tfrac{1}{2}\sigma_x u^2 X C_{d,0} \cos\phi\, dx + \underline{\int_{X_c}^{X_N} \tfrac{1}{2}\sigma_x u^2 X \left(C_{d_0} + C_{d_{mf}}\right)\cos\phi\, dx} \qquad \text{(A-28)}$$

$$C_{Q,a}(\psi) = \int_{X_c}^{X_f} \tfrac{1}{2}\sigma_x u^2 X C_\ell \sin\phi\, dx + \underline{\int_{X_f}^{X_N} \tfrac{1}{2}\sigma_x u^2 X C'_{\ell_j} \sin\phi\, dx} \qquad \text{(A-29)}$$

$$C_{Q_{Jf}}(\psi) = \underline{\int_{X_f}^{X_N} \tfrac{1}{2}\sigma_x u u_T X \cos\beta\, C'_{d_{0j}}\, dx} \qquad \text{(A-30)}$$

$$C_{Q_{mf}}(\psi) = \int_{X_f}^{X_N} \frac{1}{2} \sigma_x U U_T X \cos\beta \left(\frac{\partial C_{d_0}}{\partial \delta}\right) \delta \, dx \qquad \text{(A-31)}$$

$$C_{Q\,NOZ}(\psi) = C'_{Q\,NOZ} \cos\theta_N \qquad \text{(A-32)}$$

$$C_{P,0}(\psi) = \int_{X_c}^{X_f} \frac{1}{2} \sigma_x U^3 C_{d_0} \, dx + \int_{X_f}^{X_N} \frac{1}{2} \sigma_x U^3 \left(C_{d_0} + C_{d_{mf}}\right) dx \qquad \text{(A-33)}$$

$$C_{H,i}(\psi) = \int_{X_c}^{X_f} \frac{1}{2} \sigma_x U^2 C_L \left(-\sin\phi \sin\psi - \cos\phi \sin\beta \cos\psi\right) dx$$

$$+ \int_{X_f}^{B} \frac{1}{2} \sigma_x U^2 C'_{L_i} \left(-\sin\phi \sin\psi - \cos\phi \sin\beta \cos\psi\right) dx \qquad \text{(A-34)}$$

$$C_{H,0}(\psi) = \int_{X_c}^{X_f} \frac{1}{2} \sigma_x U^2 C_{d_0} \left(\cos\phi \sin\psi - \sin\phi \sin\beta \cos\psi\right) dx$$

$$+ \int_{X_f}^{X_N} \frac{1}{2} \sigma_x U^2 C'_{d_{0_j}} \left(\cos\phi \sin\psi - \sin\phi \sin\beta \cos\psi\right) dx \qquad \text{(A-35)}$$

$$\Delta C_{H\,NOZ}(\psi) = C'_{Q\,NOZ} \left\{ \left(\cos\theta_N \cos\phi + \sin\theta_N \sin\phi\right) \sin\psi \right.$$

$$\left. + \left(\sin\theta_N \cos\phi - \cos\theta_N \sin\phi\right) \sin\beta \cos\psi \right\} \qquad \text{(A-36)}$$

APPENDIX B

ROTOR POWER AVAILABLE (See also Ref. 12)

Introduction

The rotor power available is determined by calculating the changes in pressure and temperature of the compressed gas supplied by the engines as it travels from the engine discharge plane to the nozzles located either along the blade in the jet-flap region or at the blade tip. The state of the gas (pressure and temperature) changes under the influence of duct wall friction, centrifugal forces and heat losses. Finally, at each nozzle segment, the effective nozzle velocity is found, and the local and integrated rotor driving torque is determined and converted into rotor power.

Only the fundamentals of the thermodynamic process will be discussed in this section; the jet-flap action introduces major parameters that affect the rotor power available such as:

Flap length/blade radius

Gas split between jet-flap and tip nozzle

Mean and oscillatory deflection of jet-flap

The detailed integration of these jet-flap parameters into the Power Available determination is given in Appendix A.

Gas Condition at the Engine Exit

Within the usual helicopter flight envelope, the engine airflow, fuel flow, and pressure ratio (engine exit to inlet) form single lines when plotted on a referred basis versus the engine temperature ratio (exit to inlet). A typical plot of referred engine parameters for a fan engine is shown in Figure B-1.

With this chart, the referred airflow, $W_a \sqrt{\theta}/\delta$, referred fuel flow, $W_f/\delta\sqrt{\theta}$, and pressure ratio, P_E/P_2, are found for a selected temperature ratio, T_E/T_2. Each temperature ratio represents an engine power setting (T_E) relative to some engine inlet temperature (T_2). The takeoff and maximum continuous exit temperatures are also dependent on inlet temperature, as shown typically in Figure B-2. Various engine aerodynamic, mechanical and structural limits are involved in establishing the limits on Figure B-2; the exact details vary from manufacturer to manufacturer, but the trends are generally as shown in Figure B-2.

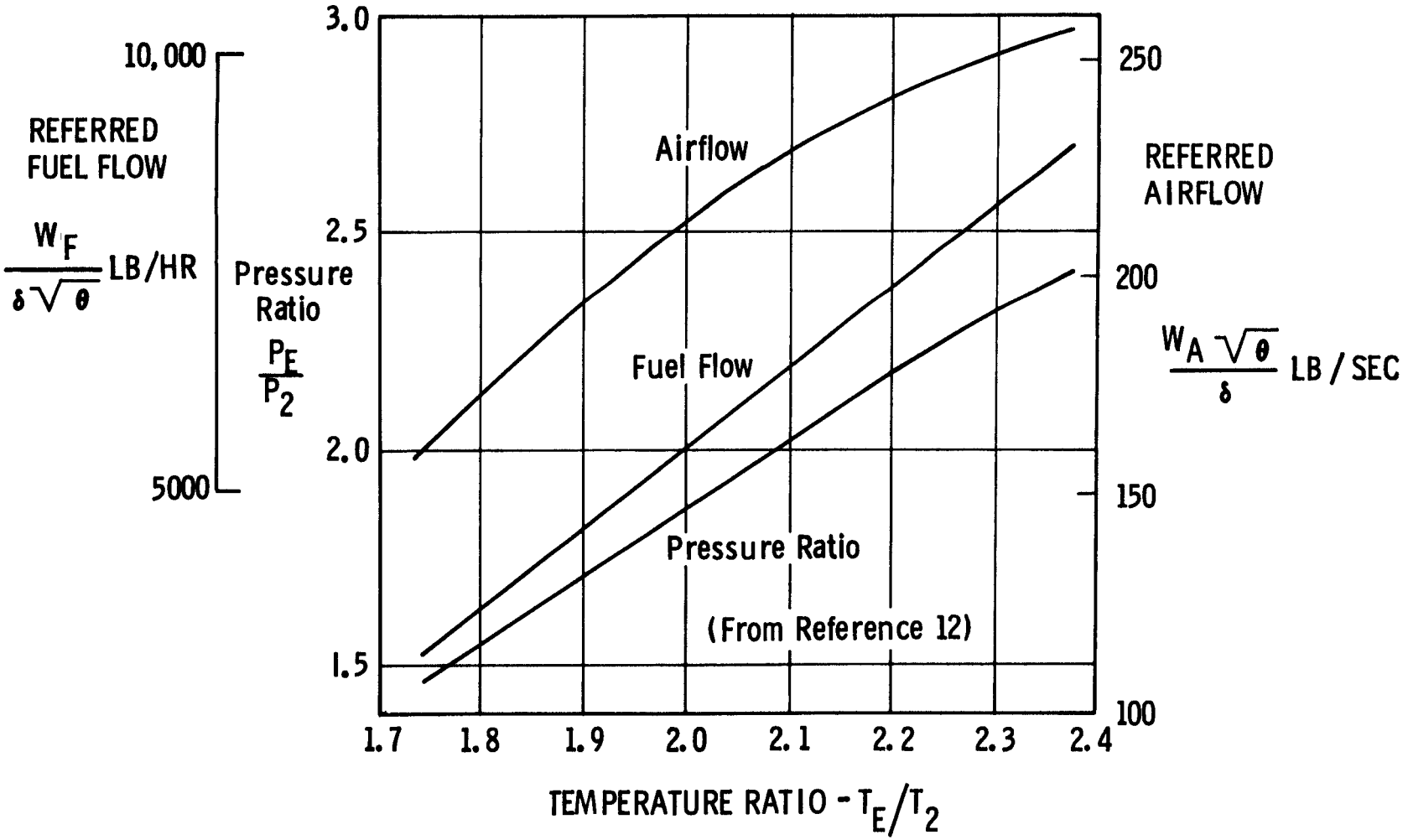

Figure B-1. Single-Line Operating Characteristics

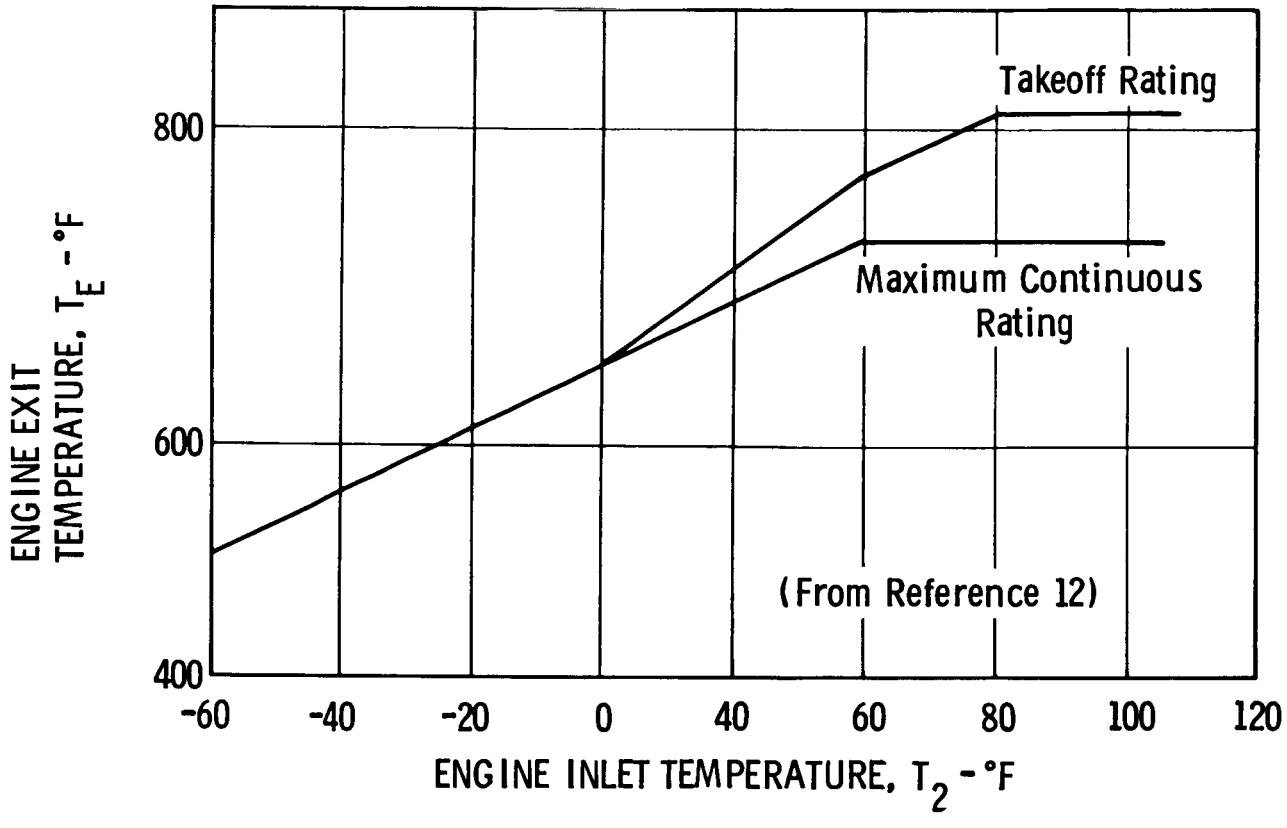

Figure B-2. Engine Exit Temperature Versus Inlet Temperature

Duct Pressure Loss from Engine to Rotor Hub

The area, the shape, and the gas path direction changes all influence the pressure loss from the engine to the rotor hub. If the average Mach Number in the ducts, plenum, and connecting elbows can be kept in the .25-.35 range, it should be possible to keep the non-blade duct pressure loss under 4% of the engine exit total pressure.

Gas Conditions along the Rotor Blade

The gas duct in the rotor blade discussed here has a duct area/blade cross-section area ratio (or utilization U) of about U = 0.73. In addition, the hydraulic diameter (D_H = 4 x area/perimeter) is approximately .18 times blade chord for a 15% thick airfoil. With these geometrical conditions, the duct slenderness ratio (R/D_H) is about 50 to 1. Further, for solidity $\sigma \simeq .11$, a blade root inlet Mach Number of about .40 is found typically for a well-proportioned rotor.

The exact equation describing the change of the gas conditions along a long rotating duct was developed by Shapiro (Reference 13) and was expanded by Henry (Reference 14) to include centrifugal forces.

The basic momentum equation is:

$$dM_D = \frac{F\, M_D(1 + KM_D^2)}{2}\,\frac{dT}{T} + \frac{2KfM_D^3}{D_H}\,dr - M_D F\,\frac{dA}{A} - \frac{-(1 + \frac{K-1}{2})\, V_T^2\, FM_D\, rdr}{g\, R_G\, TR^2} \qquad \text{where } F = \frac{(1 + \frac{K-1}{2}M_D^2)}{(1-M_D^2)} \qquad \text{(B-1)}$$

The effects on duct Mach Number are shown successively in equation B-1 for change of stagnation temperature, for effect of friction, for duct area changes, and for centrifugal forces.

Due to the insulated nature of the proposed honeycomb blades, and because of the use of added insulation to keep low bond line temperatures, the gas temperature can be expected to be perhaps $25^{\circ}R$ higher at the blade tip than at the blade root. This, coupled with the blade geometry and equation B-1, will allow calculation of the overall change of duct Mach Number.

The non-linear differential equation of Mach Number versus radius (equation B-1) can be solved with numerical integration on a computer.

The blade root Mach Number can be found knowing the gas flow, pressure, temperature, and duct area using the following equation: (Note: Subscript ""R" refers to blade root; subscript "T" refers to blade tip)

$$\frac{W\sqrt{T_R}}{P_R A_D} = \frac{M_{D_{(R)}}}{\left(1 + \frac{K-1}{2} M_{D_{(R)}}^2\right)^{\frac{K+1}{2(K-1)}}} \qquad \text{(B-2)}$$

The increment in Mach Number is found from equation B-1, and the blade tip Mach Number is defined by

$$M_{D_{(T)}} = M_{D_{(R)}} + \Delta M_D \qquad \text{(B-3)}$$

Then, knowing the duct Mach Number at the blade root and blade tip, the blade tip/blade root pressure ratio is found from the following equation:

$$\frac{P_{Tip}}{P_{Root}} = \frac{P_T}{P_R} = \frac{A_{D_R}}{A_{D_T}} \frac{M_{D_{(R)}}}{M_{D_{(T)}}} \left(\frac{1 + \frac{K-1}{2} M_{D_{(T)}}^2}{1 + \frac{K-1}{2} M_{D_{(R)}}^2}\right)^{\frac{K+1}{2(K-1)}} x\sqrt{\frac{T_T}{T_R}} \qquad \text{(B-4)}$$

Rotor Power Available

Next, the effective nozzle velocity is found by determining the isentropically expanded velocity from the local* nozzle gas total pressure and temperature, and by applying an effective nozzle velocity coefficient, C_{V_e}, which accounts for the energy which is not convertible into thrust. This coefficient is a function of the nozzle geometry (round, rectangular, etc.) and

* "local" can be at the tip nozzle or anywhere along the jet-flap.

the pressure ratio. A simple convergent nozzle was used in this study. It is expected that quite detailed analysis and test will be required to obtain the best possible gas paths for blade tip nozzles and for jet-flap nozzles. In the case of the tip nozzle, when the gas exhausts directly to the atmosphere, it appears (from recent tests of turbine nozzle vanes) that a nozzle velocity coefficient of C_{V_e} = .975 is conservative. In the case of the jet-flap, when the gas must pass over the physical flap of 0.10-0.12 times chord, frictional losses will occur, and as discussed in Reference 15b, a reduction of C_{V_e} (assumed to be .96) appears to be applicable to the jet-flap nozzle. The local jet velocity is then found from the following:

$$V_J = C_{V_e} \sqrt{2 \frac{K}{K-1} g R_G T_{local} \left[1 - \frac{P_{Amb}}{P_{local}}\right]^{\frac{K-1}{K}}} \qquad \text{(B-5)}$$

The rotor power is then determined as an integrated result of the local mass flow being ejected, the local jet velocity, the blade radius at which it is being ejected, the blade tip speed, and the helicopter forward speed. Details of this integration procedure are given in Appendix A. For illustrative purposes, the following equation is given which defines rotor power for the hovering rotor in which 100% of the gas is exhausted at the blade tip (no-jet-flap) for a hovering helicopter.

$$RHP = \frac{W_g}{g \times 550} (V_J - V_T) V_T \qquad \text{(B-6)}$$

In forward flight, ram drag of the air picked up at helicopter speed is allowed for; the ram pressure rise at the engine face partially compensates for this ram drag.

Influence of Jet-Flap on Rotor Power Available

A detailed calculation is required to determine the effects on rotor power available of the following parameters associated with use of a jet-flap:

Reduced nozzle velocity coefficient

Inboard location of average radius of jet-flap gas

Flap deflection

An approximate analysis was made of the case typical of the

Heavy-Lift Mission, where 30% of the gas is ejected uniformly along a jet-flap extending from 70 percent to 97.5 percent of blade radius, with a hover flap deflection of 40^{o}.

The approximate analysis showed that 92% of the pure tip nozzle power would be developed, based on a thrust recovery factor* of 0.5, and the detailed calculation (per Appendix A) showed 90% of reference tip nozzle power.

The flap length and flap deflection of the high speed, 2g mission was found typically to be similar to the Heavy-Lift Mission values. However, 100% of the gas is ejected along the jet-flap (none to the tip nozzle). The approximate analysis showed rotor power available to be 80% of the reference pure tip nozzle power, and the typical detailed (computer) calculation showed about 74% of reference nozzle power.

* as defined by the term S_d, supercirculation thrust parameter in Reference 5, and discussed in Appendix C.

APPENDIX C

JET-FLAP AERODYNAMIC CHARACTERISTICS

Lift Coefficient vs Momentum Coefficient

Review of literature on the aerodynamic characteristics of jet-flaps indicates that the basic data was obtained from the French work L. Malavard, et.al., Reference 15a. The data presented in Reference 15a was used to derive the lift coefficient of a deflected flap.

The equation for the lift coefficient of an airfoil with a jet-flap with blowing on the upper surface of a mechanical flap is equal to:

$$C_\ell = C_{\ell_o} + C_j \sin(\alpha + \delta) + S_\ell C_j \sin(\alpha + \delta) \qquad \text{(C-1)}$$

The first term is the lift coefficient of the basic airfoil section, the second term is the jet reaction increment, and the last term is the super-circulation increment. The data shown in Figure 25 of Reference 15a (shown herein as Figure C-1) was used to estimate S_ℓ. The value of 5.7 fits the data for the upper surface jet and the flap length of 12.5% chord. The airfoil used in this study for the baseline Warm Cycle no-jet-flap helicopter was the NACA 0015 section. C_{ℓ_o} for the basic airfoil is obtained from wind tunnel data of the NACA 0015 airfoil, Reference 11. This reference presents section C_ℓ and C_d as a function of Mach Number and angle of attack.

Section Drag Coefficient

The section drag coefficient of the airfoil with a jet-flap is equal to:

$$C_d = C_{d_o} - C_j \cos(\alpha + \delta) - S_d C_j \left[1 - \cos(\alpha + \delta)\right] + C_{d_{MF}} \qquad \text{(C-2)}$$

where C_{d_o} is the drag coefficient of the basic 15% thickness airfoil, S_d is the thrust recovery factor assumed to be equal to 0.5 for this study, and $C_{d_{MF}}$ is the drag coefficient due to the deflection of the 12.5% mechanical flap. The drag coefficient of

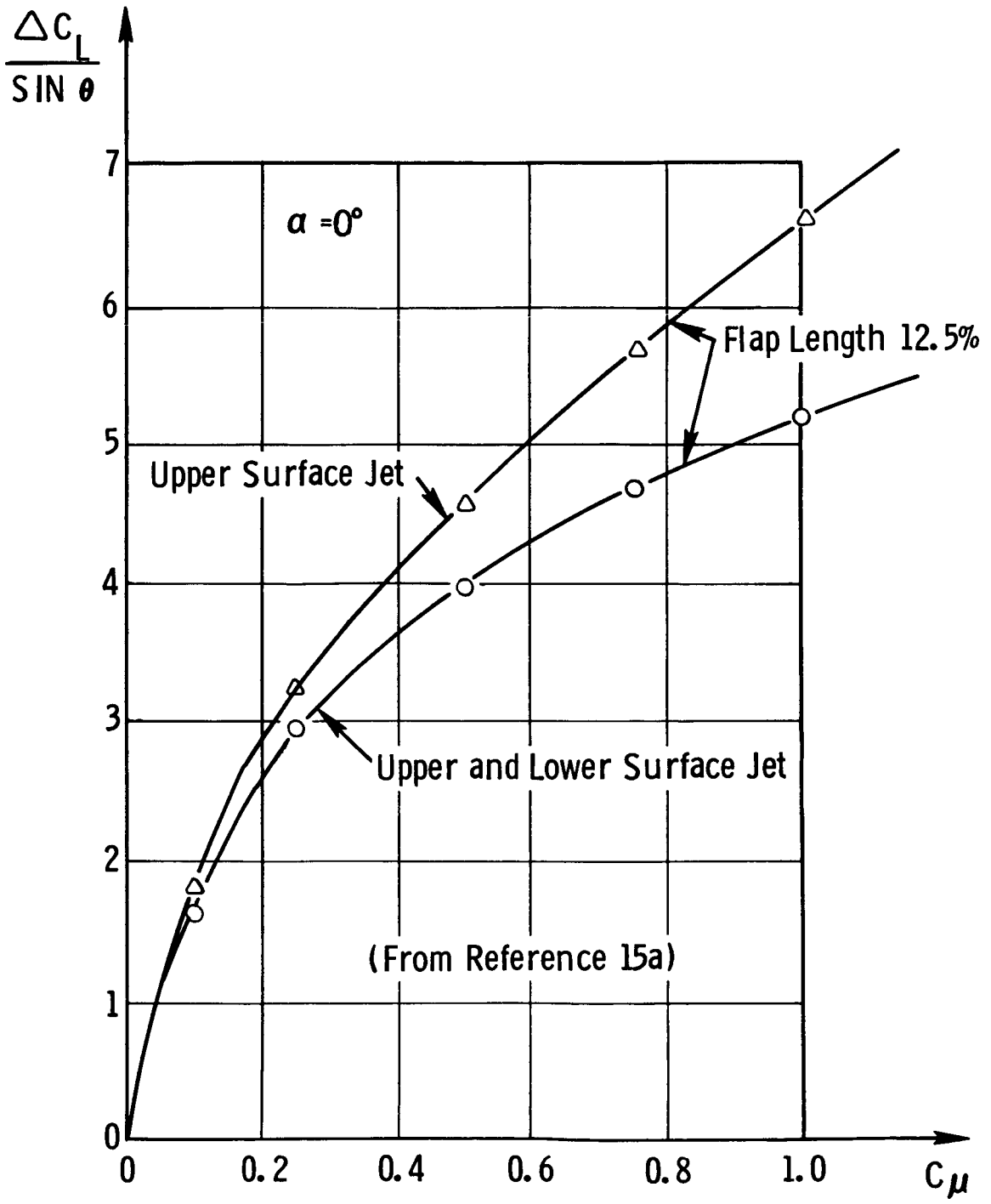

Figure C-1. Lift Variation with Blowing Over 12.5 Percent Chord Flap

the mechanical flap is equal to 0.003 δ_{flap} (Reference 16). Flight tests have indicated that the profile drag of a practical 15% thick airfoil section is approximately 7% greater than shown by Reference 11. Therefore, the profile drag terms are increased by a profile factor of 1.07 for a constant 15% thick airfoil.

Stall Angle of Attack and Drag Rise

Figure 27 of Reference 15a (shown herein as Figure C-2) shows that the angle of attack for blade stall (defined as $\alpha_{C_{L_{max}}}$) of a jet-flap airfoil is a function of jet deflection. The data shown in Figure C-2 is for symmetrical blowing on a jet-flap and C_j of 1.0. Figure 13 of Reference 15a (Figure C-3 herein) shows the effect of blowing on stall angle of attack for trailing edge blowing, at a jet deflection angle of 55 degrees; the stall angle of attack is seen to decrease with C_j for C_j = 0.4 - 1.2. Comparable data is available for moderate blowing (C_j = 0.0 - 0.158) on the upper surface of a mechanical flap in Reference 15h. Therefore, it will be assumed that stall angle will decrease for C_j between 0.2 and 1.0, when blowing over a mechanical flap, and specifically the angles for stall will be obtained from Figure C-2. These may be considered slightly conservative due to the fact that the retreating tip C_j for both the Heavy-Lift and high-speed helicopters is less than 1.0.

Based on Figures C-2 and C-3, Figure C-4 presents section stall angle of attack as a function of jet orientation angle, δ. C_ℓ is considered constant for section angles of attack greater than the stall value shown in Figure C-4. In addition, drag rise due to stall is conservatively accounted for by setting the thrust recovery to zero when the section angle of attack is above stall. It should be noted that there is an apparent lack of drag data for a jet-flap airfoil past stall. This item could be a very useful subject of future wind tunnel testing. Figure C-4 also presents values of $C_{L_{max}}$ versus C_j and δ, using equation C-1 and stall angle shown on Figure C-4. It is seen that the jet deflection angle for $C_{L_{max}}$ is in the range of 40^o - 50^o for C_j = .1 to 1.0.

Limit Angle of Attack

Roughness data obtained from flight tests at HTC have indicated that the retreating tip angle limit for roughness (V_R) occurs at

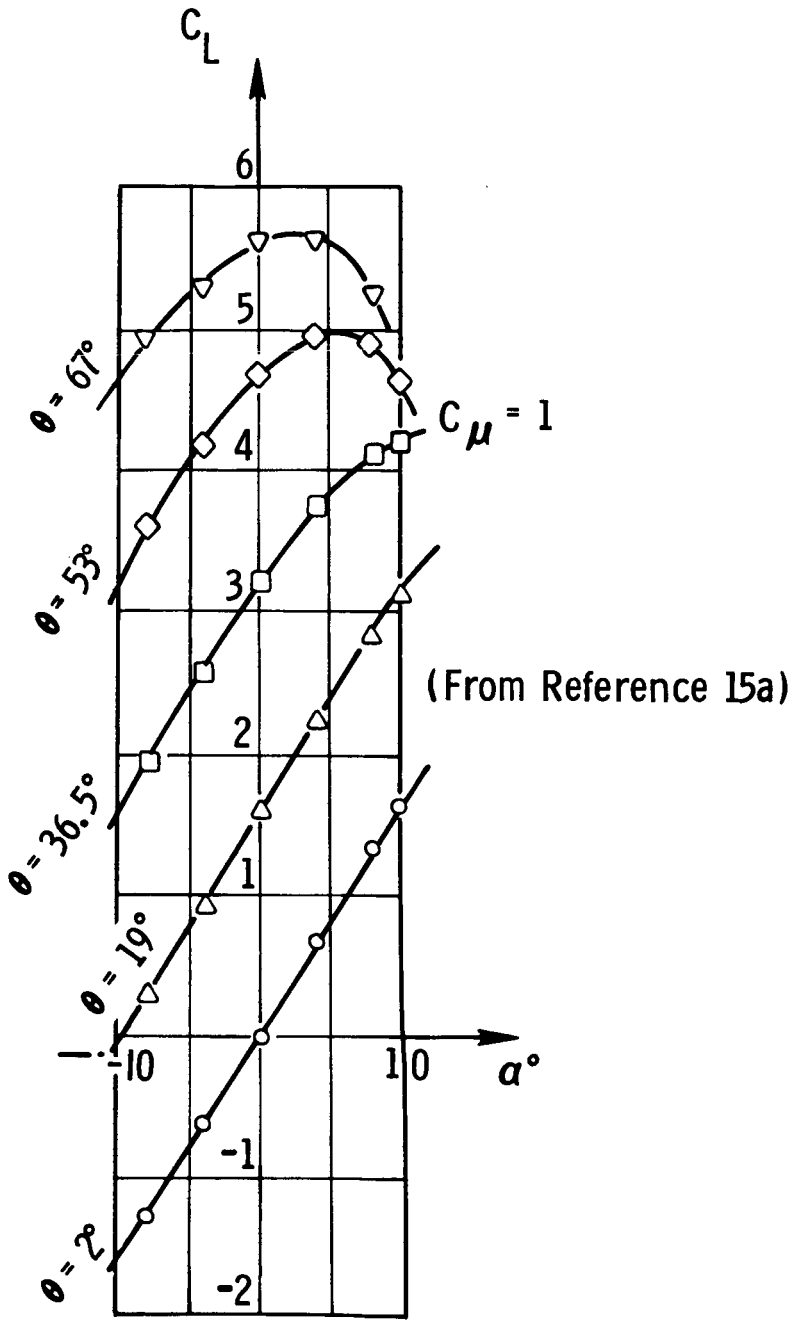

Figure C-2. Lift Coefficient Versus Angle of Attack and Jet Deflection

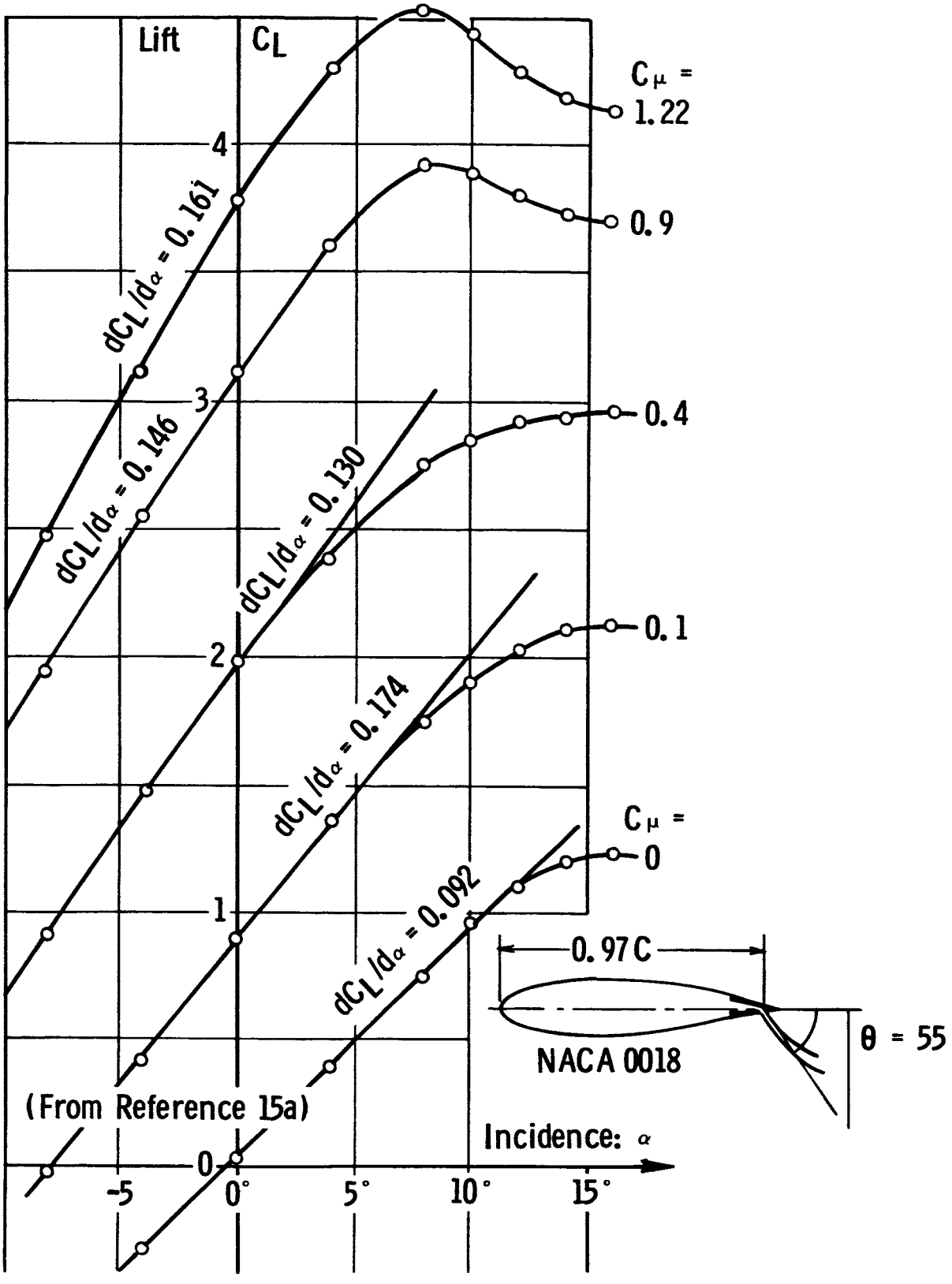

Figure C-3. Lift Coefficient Versus Angle of Attack and Momentum Coefficient

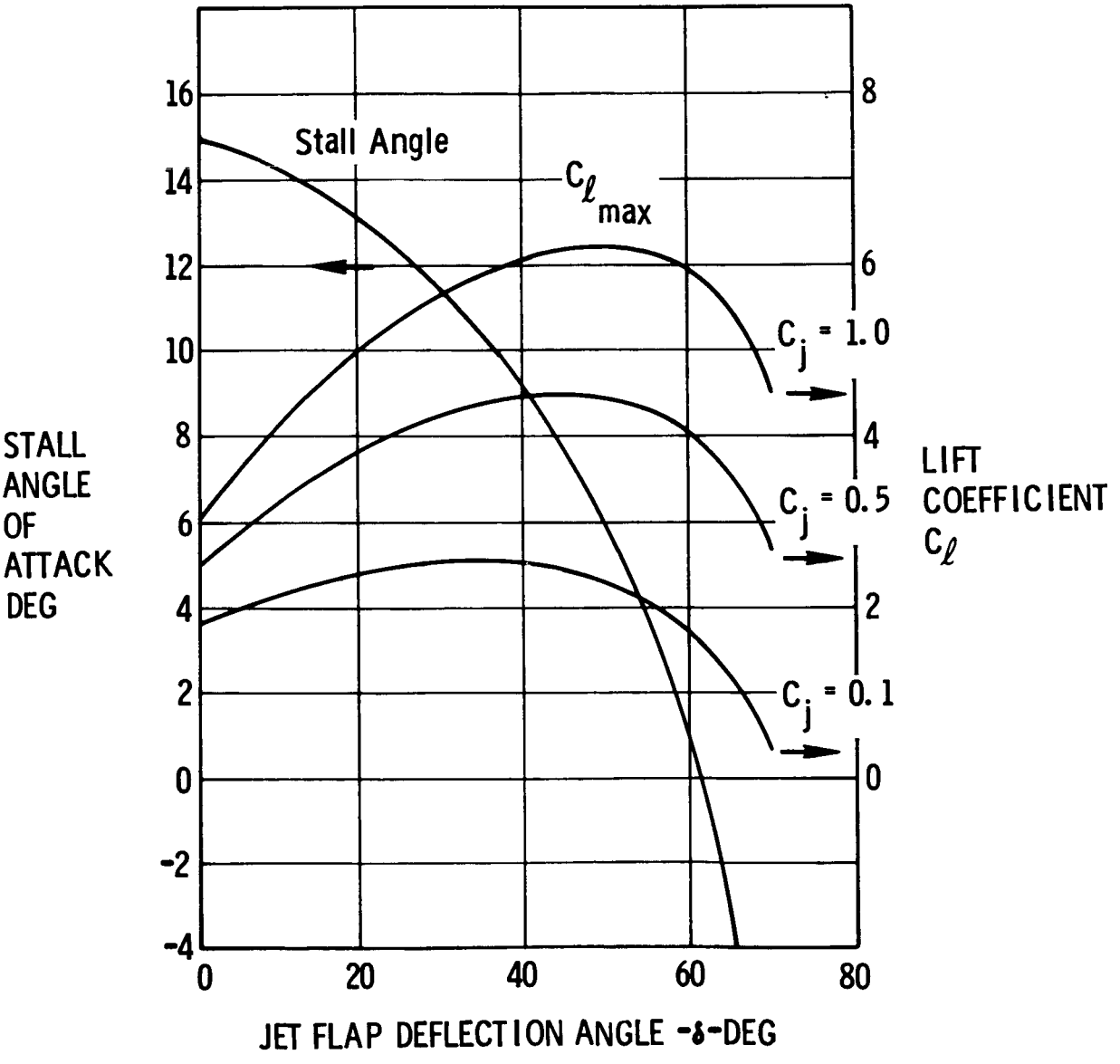

Figure C-4. Jet Flap Stall Angle and C_{ℓ} max Versus δ and C_j

approximately 2 degrees beyond 2-dimensional stall. The Heavy-Lift helicopter can cruise at V_{NE}, which is defined as 90% of roughness speed. For V_{NE}, the retreating tip angle is 1.5 degrees beyond 2-dimensional stall. The high-speed helicopter performs a 2-g maneuver at 200 knots; because of the limited duration of this maneuver, the retreating tip angle can reach the roughness value of 2 degrees beyond the stall limit. The $\alpha_{(1.0)(270)}$ margin shown refers to Figure C-4. Positive values show retreating tip limit angles less than the limit of Figure C-4 and negative values are for angles greater than Figure C-4. All angles shown are for sea level, 95°F.

Thickness Effects on Drag

Airfoils thicker than 15% are required to provide enough duct area for the Heavy-Lift jet-flap helicopters. This increased thickness applies from the blade root to the start of the jet-flap. The blade thickness of the flapped section is reduced linearly to achieve 15% at the blade tip. Reduction of the airfoil thickness in the flap section is made possible by the fact that the duct area is reduced as the air is bled off for the jet-flap. Since the penalties of drag divergence and stall occur on the tip sections of the blade, they are properly accounted for by the airfoil section characteristics of the 15% airfoil. The thicker inboard sections are at low values of Mach Number and the increase in drag can be accounted for by multiplying the profile drag terms by a weighted factor, derived as follows:

The ratio of profile drag of a thicker section to a 15% thick section can be obtained from equation 6, Chapter 6, Reference 17. The inboard section is assumed to extend to 85% of the radius while the jet-flap section started at from 65% to 75% for the cases investigated. This was done to account for the linear transition from inboard thickness to tip thickness over the flap length. The weighted factor was obtained by integrating from root to tip using the following equation:

$$PPF_{weighted} = PPF_{root\ t/c} \int_{0}^{.85} x^3 dx + PPF_{tip\ t/c} \int_{.85}^{1.0} x^3 dx \qquad (C\text{-}3)$$

This resulted in PPF = 1.14 for 20% inboard thickness and PPF = 1.17 for 22% inboard thickness with 15% outboard thickness for both cases.

APPENDIX D

EMPTY WEIGHT DETERMINATION

Introduction

The empty weights of the helicopter studied here were based on the standard use of empirically-derived statistical weight equations for the several components involved. Two sets of equations are presented here, one for the Heavy-Lift mission, and one listing the revisions to the Heavy-Lift equations to provide for the high speed mission. A common set of symbols is used.

Heavy-Lift mission.- The following equations are used for calculation of helicopter component weights:

Main Rotor Group

$$W_r = K_{jf} K_{mr} \left[1.0427\, b\, (RC)^{.879} W_g^{.231} + 2.413 \times 10^{-3}\, b^{1.067}\, (RC)^{.938} W_g^{.246} V_t^{.706} + 200 \right] \quad \text{(D-1)}$$

where K_{jf} = 1.1 (with jet-flap)

= 1.0 (no-jet-flap)

K_{mr} = .92 (Cold Cycle)

= 1.00 (Warm Cycle)

= 1.10 (Hot Cycle)

Tail Surfaces

$$W_{ts} = 2.55\, K_{ts} S_{ts} \quad \text{(D-2)}$$

where K_{ts} = .70

$$S_{ts} = .221 \left(\frac{W_g}{W_{g_b}} \right)^{2/3}$$

Tail Rotor

$$W_{tr} = 3.70\, K_{tr}\, (RCb)_{tr}^{1.213} \quad \text{(D-3)}$$

where: $K_{tr} = .90$

$$(RCb)_{tr} = 17.98 \left(\frac{W_g}{W_{g_b}}\right)$$

Body Group (fuselage)

$$W_B = .0819\ K_B W_g{}^{.611} S^{.551} \qquad \text{(D-4)}$$

where: $K_B = .75$

$$S = 1549 \left(\frac{W_g}{W_{g_b}}\right)^{2/3}$$

Alighting Gear

$$W_{lg} = 8.344 \times 10^{-3}\ K_{lg}\ W_g{}^{1.169} \qquad \text{(D-5)}$$

Flight Controls

$$W_{fc} = K_{fc}\ \ 4.84\ (RCb)^{.460} W_g{}^{.242} + 180 \qquad \text{(D-6)}$$

where: $K_{fc} = .90$

Nacelles

$$W_{nac} = .05\ W_{eng} + 43.31\ K_{nac} W_{eng}{}^{.24}\ N_e \qquad \text{(D-7)}$$

where: $K_{nac} = .80$

Engine Installation

$$W_{eng} = 1.10\ W_{re} N_e P_{air} \qquad \text{(D-8)}$$

Air Induction and Filters

$$W_{ai} = .00906\ N_{eng} N_e \qquad \text{(D-9)}$$

Exhaust System

$$W_{es} = .223\ W_{eng}^{.50}\ N_e \qquad \text{(D-10)}$$

Lubrication System (included in APU weight) (D-11)

Fuel System (fuel based on 4-trip endurance mission $= W_f$)

$$W_{fs} = 295 + 70.6\ N_t + .0614\ W_f \qquad \text{(D-12)}$$

Engine Controls and Starter (fixed propulsion systems)

$$W_{fp} = 60 + 60\ N_e \qquad \text{(D-13)}$$

Jet-Drive System

$$W_{jd} = .0888 K_{div} D_e^{2.32} N_e + 5.136\ D_e N_e + 22.64\ D_e N_e^{.50} \qquad \text{(D-14)}$$

where: Subscript "g" denotes conditions at exit of diverter valve ($K_{div} = .95$)

W_g = Gas flow/engine

N_e = number of engines

D_e = diverter valve exit diameter (in.)

$$D_e = 2\left[\left(\frac{W_g \sqrt{T_e}}{P_e}\right)_{des} \frac{1}{\pi \Gamma}\right]^{1/2}$$

The flow function $\Gamma = \left(\frac{W_g \sqrt{T_e}}{A_D P_e}\right)$ is a function of the duct Mach Number and specific heat ratio. The relationship between the internal flow loss and the diverter valve weight is determined by the choice for the flow Mach Number. A flow function of .178 (Mach Number = .2) has been found to produce a good compromise between weight and pressure losses.

NOTE: $(\ )_{des}$ denotes takeoff rating at hover design conditions.

Yaw Fan/Rotor Drive System + Accessory Gearbox

$$W_{yfd} = 25.19\ K_{yfd}\ (RCb)_{tr}^{.847} \qquad \text{(D-15)}$$

where: $K_{yfd} = .894$

Rotor Brake

$$W_{rb} = 200 \text{ lbs (constant)} \qquad \text{(D-16)}$$

Auxiliary Propulsion Group

$$W_{apu} = 506 \text{ lbs (constant)} \qquad \text{(D-17)}$$

Instruments

$$W_{i} = 400 \text{ lbs (constant)} \qquad \text{(D-18)}$$

Hydraulics and Pneumatics Group

$$W_{h} = .835\ K_{h} W_{fc}^{.740} \qquad \text{(D-19)}$$

where: $K_{h} = .90$

Electrical Group

$$W_{el} = 3.86\ K_{el} W_{g}^{.473} \qquad \text{(D-20)}$$

where: $K_{el} = .90$

Avionics

$$W_{av} = 1280 \text{ lbs (constant)} \qquad \text{(D-21)}$$

IR Countermeasures Device

$$W_{ir} = 500 \text{ lbs (constant)} \qquad \text{(D-22)}$$

Armor

$$W_{arm} = 560 \text{ lbs (constant)} \qquad \text{(D-23)}$$

Crew/Passenger Furnishings and Equipment

W_{fe} = 1000 lbs (constant) (D-24)

Airconditioning Group

W_{ac} = 350 lbs (constant) (D-25)

Anti-Icing Group

W_{an} = 100 lbs (constant) (D-26)

Auxiliary Gear (Cargo Handling Devices)

$W_{ag} = .03418\ W_{11}$ where: W_{11} = load lifted (lbs) (D-27)

Weight Empty

W_e = equations D-1 through D-27

Useful Load (W_{ul})

a. Crew @ 240 lbs/man x 5 = 1200 lbs (D-28)

b. Oil @ 17.5 lbs/engine x N_e (D-29)

c. Unusable Fuel @ .01 W_{fuel} (primary mission) (D-30)

d. Miscellaneous Equipment = 1000 lbs (constant)

e. Fuel (usable) primary mission (as required) = W_{fuel}

f. Payload 60,000 lbs

Gross Weight (Wg)

$$W_g = W_e + W_{ul} = \frac{T}{1+DWN} + \text{Warmup Fuel}$$

Revision to Heavy-Lift weight equations for high speed mission.

Body Group

$$W_B = .126\ K_B\ W_g^{.611}\ S^{.551}$$

where: $S = 920\ ft.^2$

$$W_B = 5.41\ K_B W_g^{.611}$$

Flight Controls

$$W_{fc} = 4.84\ K_{fc}\ (RCb)^{.460} W_g^{.242}$$

Nacelles

$$W_{nac} = .05\ W_{eng} + 1.847\ W_{eng}^{.67}\ N_e^{.33}\ K_{nac}$$

Engine Controls (Fixed propulsion)

$$W_{fp} = 20 + 10\ N_e$$

Rotor Brake

$$W_{rb} = 30 \text{ lbs. (constant)}$$

Auxiliary Propulsion

$$W_{apu} = 100 \text{ lbs. (constant)}$$

Instruments

$$W_i = 150 \text{ lbs. (constant)}$$

Avionics

$$W_{av} = 400 \text{ lbs. (constant)}$$

I.R. Countermeasures Device

$$W_{ir} = 300 \text{ lbs. (constant)}$$

Armor

$$W_{arm} = 500 \text{ lb. (constant)}$$

Crew/Passenger Furnishings & Equipment

$$W_{fe} = 15 \times 20 = 300 \text{ lb. (constant)}$$

Air Conditioning Group

100 lb. (constant)

Anti-Icing Group

30 lb. (constant)

Auxiliary Gear

0 lbs.

Fuel System

$$W_{fs} = \frac{2500}{14400} W_f = .174 W_{fuel}$$

Unusable Fuel

$$W_{uf} = .005 W_{fuel}$$

Miscellaneous Equipment

0 lbs.

Crew

2 men at 240 = 480 lb. (constant)

Oil

35 lb. (constant)

Payload

6000 lbs.

APPENDIX E

OPTIMIZATION PARAMETERS

It is noted on pages 12 and 22 that the block speed in the subject study is constant. Therefore, the Productivity parameter is the same as Payload/Empty Weight. Lengthy cost studies of ten-year life-cycle costs of heavy lift helicopters have been made based on source data such as Reference 18. It was found that (neglecting such relatively constant items as initial development, flight crew pay, and travel), fuel costs represent less than six percent of the ten-year costs. The other ninety-four percent of costs are proportional to empty weight at a fixed payload, or to payload/empty weight. Thus it is easy to show that the choice of Productivity (as defined on page 21) as the criterion for comparison is the correct parameter.

As confirmation of the validity of selecting a productivity criterion rather than a fuel/payload criterion as the optimization parameter, Tables E-1 and E-2 below (which are based on Tables 4 and 5 on pages 27 and 30) give the trade-off of Productivity, Fuel/Payload, and Relative Total Variable Life Cycle Costs as a function of duct Mach Number and disk loading, respectively.

TABLE E-1

EFFECT OF DUCT MACH NUMBER

Duct Mach Number	0.31		0.43*	
		Relative Cost Factor		Relative Cost Factor
Productivity	(127.4)	.966	(130.4)	.944
Fuel/Payload	(.2081)	.053	(.2198)	.056
Total Variable Life Cycle Costs		1.019		1.000

* Mach No. for highest productivity

TABLE E-2

EFFECT OF DISK LOADING

Disk Loading-lb/ft^2	7		9**	
		Relative Cost Factor		Relative Cost Factor
Productivity	(129.7)	.949	(130.4)	.944
Fuel/Payload	(.2046)	.052	(.2198)	.056
Total Varibable Life Cycle Costs		1.001		1.000

** Disk Loading for highest productivity

To prepare Tables E-1 and E-2, the values of Productivity and Fuel/Payload were noted from Tables 4 and 5 respectively, at the duct Mach No. (.43) and disk loading (9 lb/ft^2) which showed the highest productivity in the noted tables. Based on studies prepared from Reference 18, a relative cost of .944 was assigned to Productivity and a relative cost of .056 was assigned to Fuel/Payload (total = 1.000). Then the Productivity and Fuel/Payload were noted from Tables 4 and 5 for the duct Mach No. and disk loading which gave the lowest Fuel/Payload in the referenced Tables. The relative costs associated with changed productivity and Fuel/Payload were determined by multiplying the original relative costs by the ratios of Productivity and Fuel/Payload, respectively, as follows for duct Mach No. = 0.31.

Productivity: $\text{Revised cost} = .944 \times \frac{130.4}{127.4} = .966$

Fuel/Payload: $\text{Revised cost} = .056 \times \frac{.2081}{.2199} = .053$

For the duct Mach Number reduction in Table E-1 there is a 5.3% reduction of fuel/payload versus a 2.3% reduction in Productivity. For the disk loading reduction in Table E-2 there is a 7% reduction in fuel/payload versus a 0.5% reduction in productivity.

However, because of the greater influence of Productivity, it is seen that the variable life cycle costs would have been higher in both the case of optimizing disk loading or of optimizing duct Mach Number by the use of lowest fuel/payload instead of highest productivity.

APPENDIX F

SELECTION OF NUMBER OF BLADES FOR BASELINE VEHICLE

A brief study was made of the possibility of using a three-bladed rotor for the reference Warm Cycle helicopter without a jet-flap. It was found that a higher Productivity (115.5) could be obtained, essentially because the three-bladed rotor is not as constrained by duct area requirements as the four-bladed rotor, which had a Productivity of 108.8 (Figure 5). However, the individual blades of the three-blade rotor are wider and, therefore, deeper than those for a four-bladed rotor. The ratio of blade radius/spar depth (R/t), which is the basic parameter influencing blade bending frequency, is 80 for the three-blade rotor and 90 for the four-blade rotor. A lower (R/t) ratio signifies a stiffer blade. As a result, for equal disk loading and/or gross weight, the three-blade rotor first mode flapwise bending frequency is higher than that of the four-blade rotor, and will approach 3 per rev, thus increasing the possibility of high 3/rev blade bending stresses. Consequently, the four-blade rotor design was used for a no-jet-flap reference because of the lower blade bending frequency. It should also be noted that the blade radius/spar depth ratio (R/t) for the three-blade Hot Cycle jet-flap rotor (with its substantially narrower chord) is 97, leading to an acceptable blade bending frequency.

REFERENCES

1. Anon: Jet-Flap Rotor Preliminary Application Study. Vought Aeronautics Division, LTV Aerospace Corporation. Volume I - Summary Report, N69 - 25567; Volume II - Analysis Report N69 - 25568, 7 February 1969.

2. Smith, H.G., and Sullivan, R.J.: Rotor Blade Design for a Fan-Jet-Powered Heavy-Lift Helicopter. Paper presented at National Aeronautic and Space Engineering and Manufacturing Meeting. Society of Automotive Engineers (Los Angeles, California), 6-10 October 1969.

3. Gessow, A, and Crim, A.: A Method for Studying the Transient Blade-Flapping Behavior of Lifting Rotors at Extreme Operating Conditions. NACA TN-3366, 1955.

4. Gessow, A.: Equations and Procedures for Numerically Calculating the Aerodynamic Characteristics of Lifting Rotors. NACA TN-3747, 1956.

5. Evans, W.T., and McCloud, J.L.,III: Analytical Investigation of a Helicopter Rotor Driven and Controlled by a Jet-Flap. NASA TN-D-3028, 1965.

6. Fradenburgh, E.A.: Aerodynamic Efficiency Potentials of Rotary Wing Aircraft. Proceedings of the 17th Annual National Forum, The American Helicopter Society. (Washington, D.C.),17 May 1960.

7. Krebs, R.W., and Miller, W.S.: Analysis of a Pressure Jet Power Plant for a Helicopter. NACA RM E54L23, 1955.

8. McCloud, J.L.,III, and Evans, W.T.: Performance Characteristics of a Jet-Flap Rotor. Proceedings of the Conference on V/STOL and STOL Aircraft. NACA SP-116, 1966, pp 29-40.

9. Tanner, W.H.: Charts for Estimating Rotor Performance in Hover and at High Forward Speeds. NACA CR-114, 1964.

10. Finnestead, R., Conner, W., and Bass, W.: Engineering Flight Test AH-1G Helicopter (HUEY COBRA) Phase D, Part 2 Performance. Addendum. Final Report USAASTA Report on USATECOM Project No. 4-6-0500-01, March 1971.

11. Shivers, J.P., and Carpenter, P.: Effects of Compressibility on Rotor Hovering Performance and Synthesized Blade-Section Characteristics Derived from Measured Rotor Performance of Blades Having NACA 0015 Airfoil Tip Sections. NACA TN 4356, 1958.

12. Bachmann, B.: Power Available Calculation Procedure and Operational Aspects of a Tipjet - Propelled Rotor System. Paper presented at 26th Annual National Forum American Helicopter Society (Washington, D.C.), June, 1970.

13. Shapiro, A.H.: The Dynamics and Thermodynamics of Compressible Fluid Flow. The Ronald Press Company, 1953.

14. Henry, J.R.: One-Dimensional, Compressible, Viscous Flow Relations Applicable to Flow in a Ducted Helicopter Blade. NACA TN-3089, 1953.

15a. Malavard, L., Jousserandot, P., and Poisson-Quinton, P.: Jet-Induced Circulation Control. Aero Digest , Vol. 73, Nos. 3-5, September, October, November, 1956.

15b.* Korbacher, G.K., and Sridhar, K.: A Review of the Jet-Flap University of Toronto Institute of Aerophysics Report UTIA Review No. 14, May, 1960.

15c. Spence, D.A.: The Lift Coefficient of a Thin, Jet-Flapped Wing. Proceedings of the Royal Society, Vol. 238, 1956 pp 46-68.

15d. Dike, D.T., Dunn, H.S., Hazen, D.C., and Lehnert, R.F.: A Study of the Low Speed Aerodynamic Characteristics of High-Lift Flow Controlled Profiles and Wings. Aeronautical Engineering Report 349, Princeton University, 1958.

15e. Spence, D.A.: The Lift on a Thin Airfoil with a Jet-Augmented Flap. The Aeronautical Quarterly, August, 1958. pp 287-299.

*NOTE: References 15b through 15h contain theoretical and test information on jet-flap airfoil section characteristics covering from 1956 through 1970. These references confirm the choice of Reference 15a for the scope of its data.

15f. Thomas, F.: Investigations Into Increasing the Lift of Wings by Boundary Layer Control Through Blowing. Z. Flugwiss. 10, No.2, pp 46-65, 1962 (Royal Aircraft Establishment Library Translation No. 1267)

15g. Williams, J., Butler, S.F.J., and Wood, M.N.: The Aerodynamics of Jet-Flaps. Aeronautical Research Council R.&M. 3304, 1963.

15.h Scherrer, R.: Synthesis of Future High Lift Systems. Paper presented at National Aeronautic and Space Engineering and Manufacturing Meeting. Society of Automotive Engineers (Los Angeles, California), 5-9 October 1970.

16. Abbott, I., and VonDoenhoff, A.E.: Theory of Wing Sections. Dover Publications, 1959.

17. Hoerner, S.F.: Aerodynamic Drag. Published by author, 1958.

18. Leone, M.: Heavy-Lift Helicopter System Cost Model. Hughes Tool Company - Aircraft Division Report 397-P-0001. April 1970 (Confidential)